aerospace

MDPI

Article

Fixed-Time Adaptive Sliding Mode Disturbance Observer-Based Nonsingular Fixed-Time Terminal Sliding Mode Control for Uncertain Space Robot with External Disturbance

Yanzhe Yang [1], Zhiping Chen [1], An Zhu [1,*], Xiaodong Fu [2] and Haiping Ai [1,3,*]

[1] School of Energy and Mechanical Engineering, Jiangxi University of Science and Technology, Nanchang 330013, China; 5720230232@mail.jxust.edu.cn (Y.Y.); 18720020853@163.com (Z.C.)
[2] School of Aerospace Engineering, Tsinghua University, Beijing 100084, China; fuxiaodong@mail.tsinghua.edu.cn
[3] School of Mechanical Engineering and Automation, Fuzhou University, Fuzhou 350108, China
* Correspondence: zhu_an24@sina.com (A.Z.); ahpwuhan@163.com (H.A.)

Abstract

In this paper, a nonsingular fixed-time terminal sliding mode control (NFTSMC) strategy based on a fixed-time adaptive sliding mode disturbance observer (FASMDOB) is proposed for a space robot in the presence of dynamic uncertainties and external disturbance. Firstly, based on fixed-time theory, a novel FASMDOB is designed to mitigate the impacts of the lumped disturbance including dynamic uncertainties and external disturbance, improving the robustness of the control system and utilizing an adaptive technique to reduce chattering. Additionally, compared to finite-time disturbance observers (FTDOB), FASMDOB converges estimation errors to zero within a fixed time, regardless of the information about the initial states of the system. Next, a nonsingular fixed-time terminal sliding mode (NFTSM) surface is developed for the following control system design. By replacing the high-order fractional term with a piecewise function, the singularity problem in conventional terminal sliding mode control is effectively avoided. Combining FASMDOB and NFTSM surface, a FASMDOB-based NFTSMC strategy is developed, which guarantees the fixed-time convergence of the sliding mode surface and tracking errors. Notably, the proposed NFTSMC method utilizes the arctangent function to construct the reaching law, improving the performance of the control system. Lastly, based on Lyapunov theory, the fixed-time stability of the proposed control system is rigorously proven. With several comparative simulations being conducted, the feasibility and effectiveness of the proposed FASMDOB-based NFTSMC strategy are verified and highlighted.

Keywords: space robot; fixed-time control; nonsingular terminal sliding mode; adaptive disturbance observer; dynamic uncertainties; external disturbance

Academic Editor: Xiaofeng Wu

Received: 22 April 2026
Revised: 26 May 2026
Accepted: 28 May 2026
Published: 30 May 2026

1. Introduction

Recently, with wide applications in various on-orbit tasks of space exploration such as capturing unknown objects, repairing defunct satellites and maintaining the space station, space robots are considered an effective tool in performing highly demanding missions. To guarantee the safe operation of space robots in the complex outer space, superior trajectory tracking capability is essential for space robot control systems. Therefore, the trajectory tracking issue has become one of the most essential research topics for space robots. However, unlike ground-based robots, space robot systems inevitably suffer from

the influence of non-holonomic kinetics constraints due to the microgravity environment. Consequently, the motions of the base and links adversely influence each other, causing the strong coupling in the dynamics of the space robot. Furthermore, disturbance from the external environment, such as radiation pressure, negatively impacts the performance of the space robot control system or even causes system instability. Additionally, due to the uncertain inertia parameters, dynamic uncertainties can further degrade the tracking performance of space robot control systems. Thus, strong robustness, rapid convergence speed and high tracking accuracy are critical in the space robot control system.

To achieve satisfactory tracking performance for the space robot control system, various advanced control strategies have been proposed, including proportional-integral-derivative (PID) control [1–3], optimal control [4–6], backstepping control [7–9] and sliding mode control (SMC). In these methods, SMC is considered an effective control strategy for the strong coupling system under disturbances due to its advantages such as high robustness, fast convergence speed and implementation simplicity. Based on the conventional SMC, researchers propose various works [10–12]. Ref. [10] proposes an adaptive fuzzy SMC for a 3-link manipulator, using fuzzy logic system to decrease the chattering. Ref. [11] develops a repetitive learning-based integrated SMC with output feedback for a flexible space robot. Ref. [12] develops an adaptive fractional-order super-twisting sliding mode compliance control strategy for a dual-arm space robot. However, despite the superior tracking performance of SMC, conventional SMC results in the chattering of the control inputs due to the discontinuous function embedded in control strategies. Additionally, conventional SMC only achieves asymptotic convergence of system variables, which limits its application. Therefore, to mitigate the chattering in conventional SMC and achieve finite-time convergence, terminal sliding mode control (TSMC) has been developed by researchers. By replacing the linear term in conventional SMC with a fractional-order term, TSMC improves the response speed, guaranteeing the TSMC surface reaches zero in a finite time. Consequently, the finite-time convergence of TSMC is achieved based on the finite-time theory. In Ref. [13], a recursive TSMC method is developed for manipulators, utilizing a novel sliding mode observer to compensate for external disturbance. Ref. [14] designs a fault-tolerant TSMC for flexible joint manipulators, which introduces an adaptive observer to compensate for external disturbance, dynamic uncertainties and faults. Ref. [15] develops a fuzzy second-order integral TSMC for a marine cable-driven parallel grinding robot, which utilizes fuzzy logic system to compensate for dynamic uncertainties. However, TSMC achieves finite-time convergence, while the first derivative of the fractional term in the TSMC surface results in the singularity problem; namely, when tracking errors reach zero, the TSMC surface will tend to be infinite. Therefore, to resolve this problem, researchers propose nonsingular terminal sliding mode control (NTSMC). Ref. [16] combines reinforcement learning with NTSMC, proposing a novel fault-tolerant control method for manipulators under multiple faults. Ref. [17] proposes an observer-based NTSMC for a robot with global prescribed performance, introducing an adaptive composite observer to estimate dynamic and kinematic uncertainties. In Ref. [18], a discrete NTSMC method introduces an extended Kalman filter and disturbance observer for a space robot, enhancing the robustness of the control system.

Due to the strict time windows during the on-orbit servicing tasks of the space robot, it is essential that the control systems of the space robot have fast convergence speeds. However, it is worth noting that the above TSMC methods only achieve finite-time convergence. Consequently, since the maximum convergence time of finite-time control (FTC) [19–21] extremely relies on the initial states of space robot systems, the convergence speed can be significantly slow when state variables are far from equilibrium points. To overcome this weakness, fixed-time control (FXTC) is introduced. Compared to FTC, the convergence

time of FXTC is independent of the initial states of control systems and only related to control parameters. Thus, FXTC has been considered an effective control strategy to determine the bounds of convergence time by researchers. Based on the fixed-time theory, various works have been proposed. Ref. [22] proposes a neural network-based FXTC for manipulators, which combines with a barrier Lyapunov function to realize prescribed motion constraints. Ref. [23] designs an optimal FXTC for a wheeled mobile robot. It employs the adaptive dynamic programming technique to find the numerical solution of the Hamilton–Jacobi–Bellman equation, thereby achieving the optimality of control inputs. In Ref. [24], a global event-triggered FXTC is developed for stochastic nonlinear systems, which utilizes full state constraints to achieve satisfactory tracking performance.

Due to the complex outer space such as extreme temperature and high radiation, external disturbance inevitably exists in space robot control systems, negatively impacting the stability of control systems. Additionally, dynamic uncertainties arising from mechanical wear can further cause performance degradation. Therefore, anti-disturbance capability is essential for space robot control systems. To mitigate the influences from external disturbance and dynamic uncertainties, researchers propose many control methods such as the NN method [25–27], the FLS method [28–30] and the observer method [31–33]. Among these methods, observer methods offer advantages of low computational consumption and high estimation accuracy, thereby leading to widespread applications in various control systems. Ref. [31] proposes a nonlinear disturbance observer with asymptotic convergence to compensate for the friction torque for the humanoid robot hand. Ref. [32] designs an improved extended state observer to compensate for time-varying disturbance, combining a novel resonant compensation term to enhance compensation performance. Ref. [33] proposes a finite-time super-twisting sliding mode observer to compensate for actuator faults and external disturbance. Nonetheless, the aforementioned observers only achieve asymptotic or finite-time convergence of approximation errors. Thus, based on the fixed-time theory, various fixed-time disturbance observers [34–36] are proposed. In Ref. [34], a fixed-time extended state observer is introduced to estimate the lumped disturbance for a wheel mobile robot, which converges estimation errors to zero within a fixed time. Ref. [35] proposes a uniform fixed-time second-order sliding mode observer to compensate for the lumped disturbance for manipulators. Ref. [36] proposes a fixed-time observer to estimate the lumped disturbance including additive faults, dynamic uncertainties and external disturbance. Inspired by the above works, this paper combines a fixed-time sliding mode observer and an adaptive technique, designing a fixed-time adaptive sliding mode disturbance observer (FASMDOB), which converges estimation errors to zero with a fixed time and utilizes an adaptive upgrade law to mitigate chattering in the conventional sliding mode observer.

Currently, various control methods are used in International Space Station (ISS) manipulators, including model predictive control, computed torque control and resolved motion rate control, which achieve satisfactory tracking performance in the ideal scenarios. However, the disturbances from the complex outer space are widespread in space robots, and the conventional control methods in ISS manipulators have limited capability to mitigate them. Consequently, control performance is significantly degraded. Furthermore, some control methods in ISS manipulators only achieve asymptotic convergence, whose convergence time tends to be infinite. Therefore, a novel control method with fixed-time convergence and strong robustness against disturbances is demanded. Based on the above discussion, the topics of NTSMC, FXTC and disturbance compensation are crucial and highly open in the field of space robot control, which has imperative demands for the control systems that guarantee satisfactory tracking performance in the event of external disturbance and dynamic uncertainties. To resolve these issues, a FASMDOB-based nonsingular fixed-time

terminal sliding mode control (NFTSMC) strategy with a novel reaching law is designed for a space robot under the lumped disturbance in this paper. To mitigate the negative impacts from the lumped disturbance, a novel FASMDOB is designed, which achieves the fixed-time convergence and reduces the chattering. Subsequently, based on fixed-time theory, a nonsingular fixed-time terminal sliding mode (NFTSM) surface is developed, which integrates with the piecewise function to avoid the singularity problem. Leveraging the NFTSM surface, a new arctangent function-based reaching law is proposed, improving the performance of the control scheme. Lastly, based on fixed-time Lyapunov theory, the fixed-time stability of the proposed control system is rigorously proven, illustrating that both tracking errors for the trajectory and the disturbance estimation errors converge within a fixed time. To verify and highlight the superior performance of the proposed FXTC method, several simulations are conducted, including a comparative simulation with FTC [21]. Moreover, to further demonstrate the effectiveness of the proposed FXTC method, a fixed-time NTSMC (FXTNTSMC) [37] and a fixed-time disturbance observer (FXTDOB) [21] are introduced for comparisons. Although the proposed FXTC method has achieved satisfactory tracking performance, obtaining the full states of the space robot can be challenging. Therefore, to avoid this issue, the output feedback mechanism proposed by [38] and its further research [39] will be taken into consideration in the future work, which can further enhance the performance of the proposed FXTC strategy and achieve conservatism reduction.

The main contributions of this paper are as follows:

(1) The proposed NFTSMC method converges the sliding mode surface and tracking errors to small regions with a fixed time while the maximum convergence time only relies on the control parameters, enhancing the tracking performance.

(2) To mitigate the influence of the lumped disturbance on the space robot system, this paper proposes an FASMDOB, which achieves the fixed-time convergence of disturbance approximation errors and utilizes adaptive gain to reduce the chattering.

(3) By substituting the piecewise function for the high-order fractional term in the conventional terminal sliding mode surface, the proposed NFTSMC method effectively avoids the singularity problem.

The remainder of this article is organized as follows. In Section 2, a dynamic model of a space robot and some lemmas are given. In Section 3, an FASMDOB-based NFTSMC method is designed. In Section 4, the fixed-time stability of the control system is strictly proven. In Section 5, some comparative numerical simulations are provided to highlight the feasibility and effectiveness of the proposed control strategy. In Section 6, the conclusion of this research is provided.

2. Dynamics Description

The on-orbit operation of an n-link space manipulator system is shown in Figure 1. Based on the law of momentum conservation and the Second Lagrange Equation, the dynamic model of an n-link space robot system governing the position and orientation of the payload can be derived as follows:

$$\boldsymbol{H}(\boldsymbol{q})\ddot{\boldsymbol{q}} + \boldsymbol{C}(\boldsymbol{q}, \dot{\boldsymbol{q}})\dot{\boldsymbol{q}} = \boldsymbol{\tau} + \boldsymbol{d} \tag{1}$$

In the aforementioned equations, $\boldsymbol{q} \in [\, q_1,\ q_2,\ q_3,\ \ldots,\ q_n] \in \boldsymbol{R}^n$ denotes the vector of the space manipulator's joint angle position, $\dot{\boldsymbol{q}}$ and $\ddot{\boldsymbol{q}}$ denote the velocity and acceleration of space manipulator joints, respectively. $\boldsymbol{H}(\boldsymbol{q}) \in \boldsymbol{R}^{n\times n}$ denotes the positive definite inertia matrix, $\boldsymbol{C}(\boldsymbol{q}, \dot{\boldsymbol{q}}) \in \boldsymbol{R}^{n\times n}$ denotes the matrix incorporating Coriolis and centrifugal forces, respectively. $\boldsymbol{\tau} \in [\, \tau_1,\ \tau_2,\ \tau_3,\ \ldots,\ \tau_n] \in \boldsymbol{R}^n$ denotes the column vector of control input, respectively. $\boldsymbol{d} \in [\, d_1,\ d_2,\ d_3,\ \ldots,\ d_n] \in \boldsymbol{R}^n$ represents external disturbance.

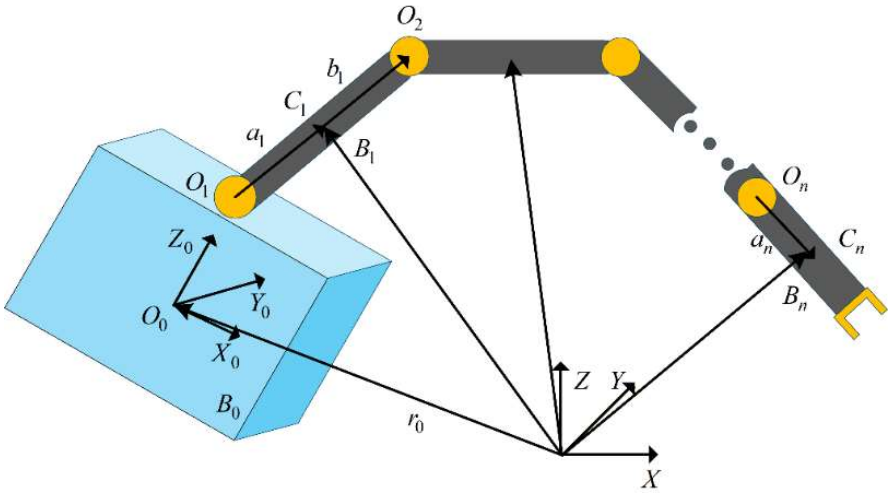

Figure 1. Model of a space manipulator.

Lemma 1 [22]. *If a class of Lyapunov function $V(x)$ for the nonlinear system $\dot{x} = f(x)$ satisfy:*

$$\dot{V}(x) \leq -\alpha V(x)^p - \beta V(x)^v + C \tag{2}$$

where $\alpha > 0$, $\beta > 0$, $p > 1$, $0 < v < 1$ and C is a positive constant, then the nonlinear system can be recognized as a practical fixed-time stable system, and the convergence time T is defined as follows:

$$T \leq \frac{1}{\alpha\eta(1-p)} + \frac{1}{\beta\eta(1-v)} \tag{3}$$

where η is a positive definite constant that satisfies $0 < \eta < 1$, and the convergence region is defined as follows:

$$\left\{ \lim_{t \to T} x \middle| V \leq \min\left\{ \left(\frac{C}{\alpha(1-\eta)} \right)^{\frac{1}{p}}, \left(\frac{C}{\beta(1-\eta)} \right)^{\frac{1}{v}} \right\} \right\} \tag{4}$$

Lemma 2 [23]. *For any positive constant $\psi_i, i = 1, \ldots, n$ and $a \in R^+$, the following inequality is obtained:*

$$\left(\sum_{i=1}^{n} |\psi_i| \right)^a \leq \max\left\{ n^{a-1}, 1 \right\} \sum_{i=1}^{n} |\psi_i|^a \tag{5}$$

3. Controller Design

In this section, the nonsingular fixed-time sliding mode (NFTSM) control strategy based on the FASMDOB for an uncertain space robot with external disturbance will be developed. First, a novel FASMDOB is introduced to deal with external disturbance and dynamic uncertainties. Subsequently, an NFTSM surface is proposed to avoid the singularity problem in the traditional fixed-time sliding mode surface. Finally, based on the proposed NFTSM surface, the NFTSM controller with arctangent function-based reaching law is developed, which enhances the performance of the proposed control strategy during the reaching phase.

3.1. Fixed-Time Adaptive Sliding Mode Disturbance Observer

Due to the fuel consumption of actuators and the extreme temperature in a complex space environment, dynamic uncertainties usually occur in kinetics model of a space robot.

Considering the mode of the space robot (1) with dynamic uncertainties, the inertia matrix $\boldsymbol{H}(\boldsymbol{q})$ and the centrifugal Coriolis matrix $\boldsymbol{C}(\boldsymbol{q}, \dot{\boldsymbol{q}})$ can be reformulated as follows:

$$\begin{cases} \boldsymbol{H} = \boldsymbol{H}_0 + \Delta\boldsymbol{H} \\ \boldsymbol{C} = \boldsymbol{C}_0 + \Delta\boldsymbol{C} \end{cases} \tag{6}$$

where $\boldsymbol{H}_0$ and $\boldsymbol{C}_0$ are the nominal parts of $\boldsymbol{H}$ and $\boldsymbol{C}$, $\Delta\boldsymbol{H}$ and $\Delta\boldsymbol{C}$ are the uncertain parts in kinetics system of the space robot.

Substituting (6) into (1), the system can be reformulated with $\boldsymbol{x}_1 = \boldsymbol{q}$ and $\boldsymbol{x}_2 = \dot{\boldsymbol{q}}$ as follows:

$$\begin{cases} \dot{\boldsymbol{x}}_1 = \boldsymbol{x}_2 \\ \dot{\boldsymbol{x}}_2 = \boldsymbol{H}_0^{-1}(\boldsymbol{\tau} - \boldsymbol{C}_0\dot{\boldsymbol{q}}) + \boldsymbol{T} \end{cases} \tag{7}$$

where $\boldsymbol{T} = \boldsymbol{H}_0^{-1}(\boldsymbol{d} - \Delta\boldsymbol{H}(\boldsymbol{q})\ddot{\boldsymbol{q}} - \Delta\boldsymbol{C}(\boldsymbol{q}, \dot{\boldsymbol{q}})\dot{\boldsymbol{q}})$ and T_i is the ith term of the lumped disturbance vector $\boldsymbol{T}$.

Assumption 1. *The lumped disturbances $\boldsymbol{T}$ is unknown and bounded within $|T_i| \leq \overline{\chi}_i, i = 1, \ldots, n$, where $\overline{\chi}_i$ is a positive constant.*

Assumption 2. *The first derivative of lumped disturbances $\dot{\boldsymbol{T}}$ is constrained within $\left|\dot{T}_i\right| \leq \chi_i$, $i = 1, \ldots, n$, where χ_i represents a positive constant.*

To design the FASMDOB for system (7), an auxiliary variable $\boldsymbol{\phi}$ is designed, which is obtained as follows:

$$\dot{\boldsymbol{\phi}} = \boldsymbol{H}_0^{-1}(\boldsymbol{\tau} - \boldsymbol{C}_0\dot{\boldsymbol{q}}) - \boldsymbol{\varpi} sig^{\delta}(\widehat{\boldsymbol{e}}) - \boldsymbol{\zeta} sig^{\boldsymbol{\vartheta}}(\widehat{\boldsymbol{e}}) - \boldsymbol{K}_a\widehat{\boldsymbol{e}} + \hat{\boldsymbol{T}} \tag{8}$$

where $\widehat{\boldsymbol{e}} = \boldsymbol{\phi} - \boldsymbol{x}_2$, the control gain $\boldsymbol{\varpi} = diag\{\varpi_1, \ldots, \varpi_n\}$, $\varpi_i > 0$, $\boldsymbol{\zeta} = diag\{\zeta_1, \ldots, \zeta_n\}$, $\zeta_i > 0$ and $\boldsymbol{K}_a = diag\{K_{a1}, \ldots, K_{an}\}$, $K_{ai} > 0$, $\boldsymbol{\delta} = [\delta_1, \ldots, \delta_n]^{\mathrm{T}}$, $\delta_i > 0$ represents a positive constant, $\boldsymbol{\vartheta} = [\vartheta_1, \ldots, \vartheta_n]^{\mathrm{T}}$ with $0 < \vartheta_i < 1$. $sig^{v}(\boldsymbol{x})$ is given as $sig^{v}(\boldsymbol{x}) = [|x_1|^{v_1}sgn(x_1), \ldots, |x_n|^{v_n}sgn(x_n)]^{\mathrm{T}}$. Subsequently, to construct FASMDOB, the fixed-time sliding mode surface of FASMDOB is given as follows:

$$\sigma_i = \dot{\widehat{e}}_i + \varpi_i\left|\widehat{e}_i\right|^{\delta_i}sgn(\widehat{e}_i) + \zeta_i\left|\widehat{e}_i\right|^{\vartheta_i}sgn(\widehat{e}_i) + K_{ai}\widehat{e}_i \tag{9}$$

Based on the fixed-time sliding mode surface (9), the FASMDOB is defined as follows:

$$\dot{\hat{T}}_i = -\alpha_{si}|\sigma_i|^{\eta_i}sgn(\sigma_i) - \beta_{si}|\sigma_i|^{\gamma_i}sgn(\sigma_i) - K_{si}\sigma_i - \hat{\chi}_i sgn(\sigma_i) \tag{10}$$

where $\alpha_{si} > 0$, $\beta_{si} > 0$ and $K_{si} > 0$ are positive constants, $\eta_i > 1, i = 1, \ldots, n$, $0 < \gamma_i < 1, i = 1, \ldots, n$.

The adaptive law of $\hat{\chi}_i$ is given as follows:

$$\dot{\hat{\chi}}_i = \mu_i(|\sigma_i| - k_{1i}\hat{\chi}_i) \tag{11}$$

where $\mu_i > 0$ denotes the learning rate and $k_{1i} > 0$ is a positive user-designed parameter.

Theorem 1. *Considering the dynamic of the space robot (7) under the lumped disturbance, the approximation errors of FASMDOB $\widetilde{\boldsymbol{T}} = \boldsymbol{T} - \hat{\boldsymbol{T}}$ can converge to small regions with a fixed time.*

Proof. Please refer to the "Appendix A". □

Remark 1. *Compared to the asymptotic and finite-time convergence disturbance observer (FTDOB), the proposed FASMDOB achieves the fixed-time convergence of approximation errors, enhancing the*

performance of the disturbance observer. Additionally, the proposed FASMDOB utilizes an adaptive technique, effectively mitigating the chattering in the conventional sliding mode observers.

3.2. Nonsingular Fixed-Time Sliding Mode Surface

Considering the singularity problem in the traditional fixed-time sliding mode controller, an NFTSM surface will be proposed in this subsection.

By defining the desired tracking trajectory $\boldsymbol{q}_d$ and its derivative $\dot{\boldsymbol{q}}_d$ the tracking errors $\boldsymbol{e}$ and the velocity errors $\dot{\boldsymbol{e}}$ are obtained:

$$\begin{cases} \boldsymbol{e} = \boldsymbol{q} - \boldsymbol{q}_d \\ \dot{\boldsymbol{e}} = \dot{\boldsymbol{q}} - \dot{\boldsymbol{q}}_d \end{cases} \tag{12}$$

Based on (12), the nonsingular fixed-time sliding mode surface is defined as follows:

$$\boldsymbol{s} = \dot{\boldsymbol{e}} + \boldsymbol{K}_1\boldsymbol{e} + \boldsymbol{K}_2 sig^{\boldsymbol{b}_1}(\boldsymbol{e}) + \boldsymbol{K}_3\boldsymbol{\Xi}_1(\boldsymbol{e}) \tag{13}$$

where $\boldsymbol{s} = [s_1, \ldots, s_n]^{\mathrm{T}}$. $\boldsymbol{K}_1 = diag\{K_{11}, \ldots, K_{1n}\}$, $\boldsymbol{K}_2 = diag\{K_{21}, \ldots, K_{2n}\}$ and $\boldsymbol{K}_3 = diag\{K_{31}, \ldots, K_{3n}\}$ are positive definite matrices and $\boldsymbol{b}_1 = [b_{11}, \ldots, b_{1n}]^{\mathrm{T}}$, $b_{1i} > 1$, $i = 1, \ldots, n$. $\boldsymbol{\Xi}_1(\boldsymbol{e}) = [\Xi_{11}(e_1), \ldots, \Xi_{1n}(e_n)]^{\mathrm{T}}$ is designed to overcome the singularity problem in traditional fixed-time sliding mode, which is derived as a piecewise function:

$$\Xi_{1i}(e_i) = \begin{cases} |e_i|^{g_{1i}} sgn(e_i) & \textbf{\textit{if}}\ \breve{s}_i = 0\ \textbf{\textit{or}}\ (\breve{s}_i \neq 0\ \textbf{\textit{and}}\ |e_i| \geq \omega_i) \\ H_{1i}e_i + H_{2i}\Psi_i(e_i)|e_i|^{g_{2i}} sgn(e_i) & \textbf{\textit{if}}\ \breve{s}_i \neq 0\ \textbf{\textit{and}}\ |e_i| < \omega_i \end{cases} \tag{14}$$

where $0.5 < g_{1i} < 1$, $1 < g_{2i} < 2$, $\Psi_i(e_i) = 1 + B_{1i}\cos(\frac{\pi e_i}{2\omega_i})$, in which $0 \leq B_{1i} < \frac{2(g_{2i}-1)}{\pi}$. $\breve{s}_i$ is derived from $\breve{s}_i = \dot{e}_i + K_{1i}e_i + K_{2i}sig^{b_{1i}}(e_i) + K_{3i}sig^{g_{1i}}(e_i)$.

Consider $\boldsymbol{\Xi}_1(\boldsymbol{e})$ is a piecewise function, thus, to guarantee the Continuity of the NFTSM surface, H_{1i} and H_{2i} are given as $H_{1i} = (g_{2i} - (\pi B_{1i}/2) - g_{1i})\omega_i^{g_{1i}-1}/(g_{2i} - (\pi B_{1i}/2) - 1)$ and $H_{2i} = (g_{1i} - 1)\omega_i^{g_{1i}-g_{2i}}/(g_{2i} - (\pi B_{1i}/2) - 1)$.

Take time derivative of the piecewise term, one can yield:

$$\dot{\Xi}_{1i}(e_i) = \begin{cases} g_{1i}|e_i|^{g_{1i}-1}\dot{e}_i & \textbf{\textit{if}}\ \breve{s}_i = 0\ \textbf{\textit{or}}\ (\breve{s}_i \neq 0\ \textbf{\textit{and}}\ |e_i| \geq \omega_i) \\ H_{1i}\dot{e}_i + H_{2i}\dot{e}_i f_{gi}(e_i) & \textbf{\textit{if}}\ \breve{s}_i \neq 0\ \textbf{\textit{and}}\ |e_i| < \omega_i \end{cases} \tag{15}$$

where $f_{gi}(e_i)$ is defined as follows:

$$f_{gi}(e_i) = \Psi_i(e_i)g_{2i}|e_i|^{g_{2i}-1} - B_{1i}\frac{\pi}{2\omega_i}\sin(\frac{\pi e_i}{2\omega_i})|e_i|^{g_{2i}}sgn(e_i) \tag{16}$$

Based on the above equations, it can be seen that the piecewise term $\dot{\Xi}_{1i}(e_i)$ is continuous when it starts to switch. Thus, since $\dot{\Xi}_{1i}(e_i)$ is continuous, the derivative of the proposed sliding mode surface is continuous, which can significantly improve the tracking performance.

3.3. NFTSM Control Strategy with a Novel Reaching Law

Based on the NFTSM surface (14), the equivalent law of the FASMDOB-based NFTSM control strategy is obtained as follows:

$$\boldsymbol{\tau}_{\text{equivalent}} = \boldsymbol{H}_0(\ddot{\boldsymbol{q}}_d - \boldsymbol{K}_1\dot{\boldsymbol{e}} - \boldsymbol{K}_2\lfloor|\boldsymbol{e}|\rfloor^{\boldsymbol{b}_1-1}\dot{\boldsymbol{e}} - \boldsymbol{K}_3\dot{\boldsymbol{\Xi}}_1(\boldsymbol{e}) + \hat{\boldsymbol{T}}) + \boldsymbol{C}_0\dot{\boldsymbol{q}} \tag{17}$$

where $\lfloor\boldsymbol{x}\rfloor^{\boldsymbol{v}}$ represents $\lfloor\boldsymbol{x}\rfloor^{\boldsymbol{v}} = diag\{x_1^{v_1}, x_2^{v_2}, \ldots, x_n^{v_n}\}$.

To enhance the performance of the NFTSM control strategy under the reaching phase, a novel reaching law based on the arctangent function is proposed:

$$\widetilde{s}_i = -K_{4i}s_i - \frac{L_{1i}}{P_i(s_i)}|s_i|^{v_{1i}}sgn(s_i) - \frac{L_{2i}}{P_i(s_i)}|s_i|^{v_{2i}}sgn(s_i) \tag{18}$$

where $K_{4i} > 0$, $L_{1i} > 0$, $L_{2i} > 0$, $0 < v_{1i} < 1$ and $v_{2i} > 1$. $P_i(s_i)$ is derived from the following:

$$P_i(s_i) = L_{3i}(\frac{\pi}{2} - \arctan(L_{4i}|s_i|^{v_{3i}})) \tag{19}$$

where $L_{3i} > \frac{2}{\pi}$, $L_{4i} > 0, 0 < v_{3i} \leq 1$.

Based on the reaching law (18), the switching law of the FASMDOB-based NFTSM control strategy is given as follows:

$$\boldsymbol{\tau}_{\text{reaching}} = \boldsymbol{H}_0(-\boldsymbol{K}_4\boldsymbol{s} - \frac{\boldsymbol{L}_1}{\boldsymbol{P}(\boldsymbol{s})}sig^{v_2}(\boldsymbol{s}) - \frac{\boldsymbol{L}_2}{\boldsymbol{P}(\boldsymbol{s})}sig^{v_3}(\boldsymbol{s})) \tag{20}$$

Combining the equivalent law (17) and reaching law (20), the proposed FASMDOB-based NFTSM controller is designed as follows:

$$\begin{aligned}\boldsymbol{\tau}_{\text{NFTSMC}} &= \boldsymbol{\tau}_{\text{equivalent}} + \boldsymbol{\tau}_{\text{reaching}} \\ &= \boldsymbol{H}_0(\ddot{\boldsymbol{q}}_d - \boldsymbol{K}_1\dot{\boldsymbol{e}} - \boldsymbol{K}_2\lfloor|\boldsymbol{e}|\rceil^{b_1-1}\dot{\boldsymbol{e}} - \boldsymbol{K}_3\dot{\Xi}_1(\boldsymbol{e}) + \hat{\boldsymbol{T}}) + \boldsymbol{C}_0\dot{\boldsymbol{q}} \\ &+\boldsymbol{H}_0(-\boldsymbol{K}_4\boldsymbol{s} - \tfrac{\boldsymbol{L}_1}{\boldsymbol{P}(\boldsymbol{s})}sig^{v_1}(\boldsymbol{s}) - \tfrac{\boldsymbol{L}_2}{\boldsymbol{P}(\boldsymbol{s})}sig^{v_2}(\boldsymbol{s}))\end{aligned} \tag{21}$$

Combining FASMDOB (8)–(11), NFTSM surface (13), NFTSM equivalent control law (17) and NFTSM reaching law (20), the control block diagram is shown in Figure 2.

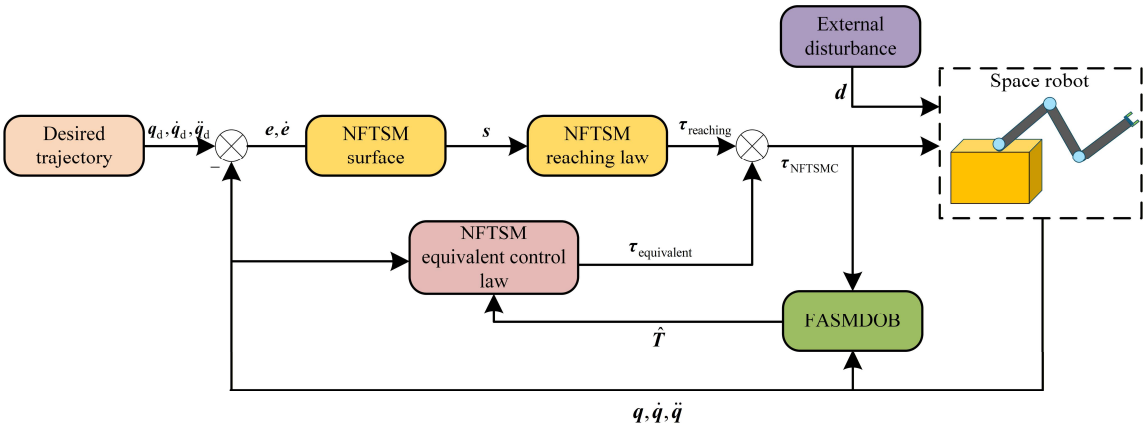

Figure 2. The diagram of the proposed controller.

Remark 2. *By using a piecewise function as a sliding mode surface, the NFTSM surface (13) effectively avoids the singularity problem. Furthermore, NFTSMC (21) is proposed, which has the following features: (1) Tracking errors can converge to the small neighbourhoods with a fixed time when the NFTSM surface reaches zero. (2) Based on the NFTSM surface, a novel reaching law (20) is proposed. Since the arctangent function is constrained between 0 and* $\frac{\pi}{2}$, $0 < P_i(s_i) < 1$ *is satisfied, resulting in the fact that* $\frac{\boldsymbol{L}_1}{\boldsymbol{P}(\boldsymbol{s})}$ *and* $\frac{\boldsymbol{L}_2}{\boldsymbol{P}(\boldsymbol{s})}$ *are larger than single* $\boldsymbol{L}_1$ *and* $\boldsymbol{L}_2$*. Thus, the stability of control systems is not affected, and the convergence speed is extremely enhanced when the sliding variable is far from zero.*

4. Stability Analysis

Theorem 2. *Considering the uncertain space robot system with external disturbance (7), FASM-DOB (10) proposed to approximate the lumped disturbances and the NFTSM controller (21) are all designed to converge tracking errors* $\boldsymbol{e}$ *into the small neighbourhoods within a fixed time, the stability proof of the proposed control system will be presented.*

Proof. The first Lyapunov function V_1 is selected as follows:

$$V_{1i} = \frac{1}{2}s_i^2 \tag{22}$$

Based on the NFTSM surface (13), one yields:

$$\begin{aligned} \dot{\boldsymbol{s}} &= \ddot{\boldsymbol{q}} - \ddot{\boldsymbol{q}}_d + \boldsymbol{K}_2 \lfloor |\boldsymbol{e}| \rceil^{b_1 - 1} \dot{\boldsymbol{e}} + \boldsymbol{K}_3 \dot{\boldsymbol{\Xi}}_1(\boldsymbol{e}) \\ &= \boldsymbol{H}_0^{-1}(\boldsymbol{\tau} - \boldsymbol{C}_0 \dot{\boldsymbol{q}}) + \boldsymbol{T} - \ddot{\boldsymbol{q}}_d + \boldsymbol{K}_1 \dot{\boldsymbol{e}} + \boldsymbol{K}_2 \lfloor |\boldsymbol{e}| \rceil^{b_1 - 1} \dot{\boldsymbol{e}} + \boldsymbol{K}_3 \dot{\boldsymbol{\Xi}}_1(\boldsymbol{e}) \end{aligned} \tag{23}$$

Taking the derivative of V_{1i}, and substituting (21) into (23), the following equality is obtained:

$$\begin{aligned} \dot{V}_{1i} &= s_i \dot{s}_i \\ &= s_i(-K_{4i}s_i - \tfrac{L_{1i}}{P_i(s_i)}|s_i|^{v_{1i}}\, sgn(s_i) - \tfrac{L_{2i}}{P_i(s_i)}|s_i|^{v_{2i}}\, sgn(s_i) + T_i) \end{aligned} \tag{24}$$

Simplified (24), one can be obtained:

$$\dot{V}_{1i} = -K_{4i}s_i^2 - \frac{L_{1i}}{P_i(s_i)}2^{\frac{v_{1i}+1}{2}}\left(\frac{1}{2}s_i^2\right)^{\frac{v_{1i}+1}{2}} - \frac{L_{2i}}{P_i(s_i)}2^{\frac{v_{2i}+1}{2}}\left(\frac{1}{2}s_i^2\right)^{\frac{v_{2i}+1}{2}} + \Pi_i \tag{25}$$

where $\Pi_i = s_i T_i$.

Considering the control parameters $\frac{v_{1i}+1}{2}$ and $\frac{v_{2i}+1}{2}$ satisfy that $\frac{v_{1i}+1}{2} > 1$ and $0 < \frac{v_{2i}+1}{2} < 1$, based on Lemma 2, one is given as follows:

$$\dot{V}_{1i} = -K_{5i}V_{1i} - L_{3i}V_{1i}^{\frac{v_{1i}+1}{2}} - L_{4i}V_{1i}^{\frac{v_{2i}+1}{2}} + \Pi_i \tag{26}$$

where $K_{5i} = 2K_{4i}$, $L_{3i} = \frac{L_{1i}}{P_i(s_i)}2^{\frac{v_{1i}+1}{2}}$, $L_{4i} = \frac{L_{2i}}{P_i(s_i)}2^{\frac{v_{2i}+1}{2}}$.

To achieve the following stability analysis, (26) can be reformulated into three forms:

$$\dot{V}_{1i} = -(1-\gamma_0)K_{5i}V_{1i} - \gamma_0 K_{5i}V_{1i} - L_{3i}V_{1i}^{\frac{v_{1i}+1}{2}} - L_{4i}V_{1i}^{\frac{v_{2i}+1}{2}} + \Pi_i \tag{27}$$

$$\dot{V}_{1i} = -K_{5i}V_{1i} - (1-\gamma_0)L_{3i}V_{1i}^{\frac{v_{1i}+1}{2}} - \gamma_0 L_{3i}V_{1i}^{\frac{v_{1i}+1}{2}} - L_{4i}V_{1i}^{\frac{v_{2i}+1}{2}} + \Pi_i \tag{28}$$

$$\dot{V}_{1i} = -K_{5i}V_{1i} - L_{3i}V_{1i}^{\frac{v_{1i}+1}{2}} - (1-\gamma_0)L_{4i}V_{1i}^{\frac{v_{2i}+1}{2}} - \gamma_0 L_{4i}V_{1i}^{\frac{v_{2i}+1}{2}} + \Pi_i \tag{29}$$

where $0 < \gamma_0 < 1$ is a positive constant.

Considering (27), when $-(1-\gamma_0)K_{5i}V_{1i} + \Pi_i \leq 0$, (27) can be transformed into the following inequality:

$$\dot{V}_{1i} \leq -\gamma_0 K_{5i}V_{1i} - L_{3i}V_{1i}^{\frac{v_{1i}+1}{2}} - L_{4i}V_{1i}^{\frac{v_{2i}+1}{2}} \tag{30}$$

Solving the differential inequality (30), it can be seen that V_{1i} converge to zero within a fixed time T_{s1}:

$$\begin{aligned} T_{s1} &\leq \lim_{V_{1i}(s_0)\to\infty} \int_0^{V_{1i}(s_0)} \frac{dV_{1i}}{\gamma_0 K_{5i} V_{1i} + L_{3i} V_{1i}^{\frac{v_{1i}+1}{2}} + L_{4i} V_{1i}^{\frac{v_{2i}+1}{2}}} \\ &\leq \int_0^1 \left(\frac{dV_{1i}}{\gamma_0 K_{5i} V_{1i} + L_{4i} V_{1i}^{\frac{v_{2i}+1}{2}}}\right) + \lim_{V_{1i}(s_0)\to\infty} \int_1^{V_{1i}(s_0)} \frac{dV_{1i}}{L_{3i} V_{1i}^{\frac{v_{1i}+1}{2}}} \\ &= \frac{2}{\gamma_0 K_{5i}(1-v_{2i})} \ln\left(1 + \frac{\gamma_0 K_{5i}}{L_{4i}}\right) + \frac{2}{L_{3i}(v_{1i}-1)} \end{aligned} \tag{31}$$

Based on (30), the convergence region for the NFTSM variable s_i is defined as follows:

$$\left\{ \lim_{t\to T_{s1}} |s_i| \leq \sqrt{2\left(\frac{\Pi_i}{K_{5i}(1-\gamma_0)}\right)} \right\} \tag{32}$$

Analyzing (28) and (29) in a similar way, the convergence time of s_i is obtained by combining different forms (27), (28) and (29):

$$T_m \leq \max\{T_{s1}, T_{s2}, T_{s3}\} \tag{33}$$

where $T_{s2} = \frac{2\ln(1+\frac{K_{5i}}{L_{4i}})}{K_{5i}(1-v_{2i})} + \frac{2}{\gamma_0 L_{3i}(v_{1i}-1)}$ and $T_{s3} = \frac{2\ln(1+\frac{K_{5i}}{\gamma_0 L_{4i}})}{K_{5i}(1-v_{2i})} + \frac{2}{L_{3i}(v_{1i}-1)}$, and the convergence region is defined as follows:

$$\Omega_{1i} = \left\{ \lim_{t\to T_m} s_i \;\middle|\; |s_i| \leq \min\left\{ \sqrt{2\left(\frac{\Pi_i}{K_{5i}(1-\gamma_0)}\right)}, \sqrt{2\left(\frac{\Pi_i}{L_{3i}(1-\gamma_0)}\right)^{\frac{2}{v_{1i}+1}}}, \sqrt{2\left(\frac{\Pi_i}{L_{4i}(1-\gamma_0)}\right)^{\frac{2}{v_{2i}+1}}} \right\} \right\} \tag{34}$$

Based on the above analysis, the NFTSM variable s_i will converge into a small neighbourhood within a fixed time T_m during the reaching phase. To guarantee that the tracking errors $\boldsymbol{e}$ converge into the small neighbourhoods within the fixed time, the following analysis is given for the sliding phase.

Define the second Lyapunov Function V_{2i} as follows:

$$V_{2i} = \frac{1}{2} e_i^2 \tag{35}$$

Since the proposed NFTSM surface s_i is a piecewise function, thus, the following analysis can be divided into three different cases: Case 1: $\breve{s}_i = 0$. Case 2: $\breve{s}_i \neq 0$ with $|e_i| \geq \omega_i$. Case 3: $\breve{s}_i \neq 0$ with $|e_i| < \omega_i$

Case 1: Based on the case that $\breve{s}_i = 0$, the NFTSM surface (13) can be expressed as follows:

$$s_i = \dot{e}_i + K_{1i} e_i + K_{2i} |e_i|^{b_{1i}} sgn(e_i) + K_{3i} |e_i|^{g_{1i}} sgn(e_i) \tag{36}$$

Since $s_i = \breve{s}_i = 0$ is satisfied in Case 1, (36) is reformed into the following:

$$\dot{e}_i = -K_{1i} e_i - K_{2i} |e_i|^{b_{1i}} sgn(e_i) - K_{3i} |e_i|^{g_{1i}} sgn(e_i) \tag{37}$$

Based on (37), taking time derivative of V_{2i}, one gets the following:

$$\begin{aligned} \dot{V}_{2i} &= e_i \dot{e}_i \\ &= e_i(-K_{1i} e_i - K_{2i} |e_i|^{b_{1i}} sgn(e_i) - K_{3i} |e_i|^{g_{1i}} sgn(e_i)) \\ &= -K_{1i} e_i^2 - K_{2i} |e_i|^{b_{1i}+1} - K_{3i} |e_i|^{g_{1i}+1} \\ &= -2K_{1i} V_{2i} - 2^{\frac{b_{1i}+1}{2}} K_{2i} V_{2i}^{\frac{b_{1i}+1}{2}} - 2^{\frac{g_{1i}+1}{2}} K_{3i} V_{2i}^{\frac{g_{1i}+1}{2}} \end{aligned} \tag{38}$$

Similar to (31), the convergence time T_{e1} of the tracking errors e_i in Case 1 is obtained as follows:

$$T_{e1} \leq \frac{2}{2K_{1i}(1-g_{1i})} \ln\left(1+\frac{2K_{1i}}{2^{\frac{g_{1i}+1}{2}}K_{3i}}\right) + \frac{2}{2^{\frac{b_{1i}+1}{2}}K_{2i}(b_{1i}-1)} \tag{39}$$

Thus, the tracking errors e_i converge into zero within a fixed time T_{e1} in Case 1.

Case 2: When $\breve{s}_i \neq 0$ with $|e_i| \geq \omega_i$, the NFTSM surface (13) can be transformed into the following form:

$$\dot{e}_i + K_{1i}e_i + K_{2i}|e_i|^{b_{1i}}\, sgn(e_i) + K_{3i}|e_i|^{g_{1i}}\, sgn(e_i) - s_i = 0 \tag{40}$$

Based on (40), the derivative of Lyapunov Function V_{2i} can be transformed into the following:

$$\begin{aligned}
\dot{V}_{2i} &= e_i\dot{e}_i \\
&= e_i(-K_{1i}e_i - -K_{2i}|e_i|^{b_{1i}}sgn(e_i) - K_{3i}|e_i|^{g_{1i}}sgn(e_i) - s_i) \\
&= -K_{1i}e_i^2 - K_{2i}|e_i|^{b_{1i}+1} - K_{3i}|e_i|^{g_{1i}+1} + e_is_i \\
&\leq -2^{\frac{b_{1i}+1}{2}}K_{2i}V_{2i}^{\frac{b_{1i}+1}{2}} - 2^{\frac{g_{1i}+1}{2}}K_{3i}V_{2i}^{\frac{g_{1i}+1}{2}} + |e_i||s_i| \\
&\leq -2^{\frac{b_{1i}+1}{2}}K_{2i}V_{2i}^{\frac{b_{1i}+1}{2}} - 2^{\frac{g_{1i}+1}{2}}K_{3i}V_{2i}^{\frac{g_{1i}+1}{2}} + |e_i|\theta_{si}
\end{aligned} \tag{41}$$

where θ_{si} satisfies $|s_i| \leq \theta_{si}$.

Based on (41) and Lemma 2, the convergence region of tracking errors e_i can be defined as follows:

$$\Omega_{2i} = \left\{ \lim_{t\to T_{e2}} e_i \,\middle|\, |e_i| \leq \min\left\{ \omega_i, \left(\frac{|e_i|\theta_{si}}{K_{2i}(1-\eta_s)}\right)^{\frac{1}{b_{1i}+1}}, \left(\frac{|e_i|\theta_{si}}{K_{3i}(1-\eta_s)}\right)^{\frac{1}{g_{1i}+1}} \right\} \right\} \tag{42}$$

where $0 < \eta_s < 1$.

From the above analysis, tracking errors will converge to the small neighbourhoods within a fixed time T_{e2}, where T_{e2} is given as follows:

$$T_{e2} \leq \frac{2}{2^{\frac{b_{1i}+1}{2}}K_{2i}\eta_s(1-b_{1i})} + \frac{2}{2^{\frac{g_{1i}+1}{2}}K_{3i}\eta_s(1-g_{1i})} \tag{43}$$

When $\breve{s}_i \neq 0$ with $|e_i| < \omega_i$, the convergence of tracking errors e_i is already included in (43). Thus, based on the above analysis, tracking error e_i will converge into a small neighbourhood within a fixed time. The proof of Theorem 2 has been achieved. □

5. Numerical Simulations

To verify the effectiveness of the designed control algorithm, a system simulation is conducted using the space manipulator model depicted in Figure 1. The following system inertia parameters are taken. As shown in Table 1.

Table 1. Inertial parameters.

Description	Symbols	Values
Mass (kg)	m_0, m_1, m_2	40.0, 4.0, 3.0
Inertia (kg·m^2)	I_0, I_1, I_2	16.67, 1.5, 1.5
Centre of mass (m)	d_0, d_1, d_2	0.5, 0.5, 0.5
Length (m)	L_0, L_1, L_2	1.0, 1.0, 1.0

The proposed simulation parameters are given as follows. As shown in Table 2.

Table 2. Control parameters.

Parameter	Value	Parameter	Value	Parameter	Value
$\boldsymbol{\varpi}$	$15I_{3\times3}$	μ_1, μ_2, μ_3	7, 4, 5	K_{41}, K_{42}, K_{43}	1, 2, 2
$\boldsymbol{\zeta}$	$15I_{3\times3}$	k_{11}, k_{12}, k_{13}	10, 10, 10	L_{11}, L_{12}, L_{13}	1, 2, 2
$\delta_1, \delta_2, \delta_3$	1.2, 1.2, 1.2	$\boldsymbol{K}_1$	$I_{3\times3}$	L_{21}, L_{22}, L_{23}	1, 2, 2
$\vartheta_1, \vartheta_2, \vartheta_3$	0.7, 0.7, 0.7	$\boldsymbol{K}_2$	$I_{3\times3}$	v_{11}, v_{12}, v_{13}	0.5, 0.5, 0.5
$\gamma_1, \gamma_2, \gamma_3$	0.7, 0.7, 0.7	$\boldsymbol{K}_3$	$I_{3\times3}$	v_{21}, v_{22}, v_{23}	1.2, 1.2, 1.2
$\boldsymbol{K}_a$	$20I_{3\times3}$	b_{11}, b_{12}, b_{13}	1.2, 1.2, 1.2	L_{31}, L_{32}, L_{33}	1, 1, 1
$\alpha_{s1}, \alpha_{s2}, \alpha_{s3}$	15, 15, 15	g_{11}, g_{12}, g_{13}	0.7, 0.7, 0.7	L_{41}, L_{42}, L_{43}	1, 1, 1
$\beta_{s1}, \beta_{s2}, \beta_{s3}$	15, 15, 15	g_{21}, g_{22}, g_{23}	1.3, 1.3, 1.3	v_{31}, v_{32}, v_{33}	0.5, 0.5, 0.5
η_1, η_2, η_3	1.2, 1.2, 1.2	B_{11}, B_{12}, B_{13}	0.3, 0.3, 0.3		
K_{s1}, K_{s2}, K_{s3}	40, 40, 40	$\omega_1, \omega_2, \omega_3$	0.05, 0.05, 0.05		

For the FASMDOB component, to balance estimation performance and chattering, we choose the control parameters that achieve a small convergence time and high approximation accuracy, while reducing the chattering from the switching function. As for the reaching law of the proposed NFTSMC, the selection of L_{1i}, L_{2i}, K_{4i} are based on the tracking performance and smoothness of control signals, mitigating overshoots of tracking errors and chattering while enhancing convergence speed. Moreover, to further balance convergence speed and chattering, L_{3i} and L_{4i} should be chosen conversely, thereby achieving a small convergence time and reduced chattering.

The desired trajectory of the space robot in the simulation is given as follows:

$$\boldsymbol{q}_d = \begin{bmatrix} 0.3\cos(t) + 0.1\sin(t) \\ 0.1\sin(t) - 0.3 \\ 0.1\sin(t) - 0.3\cos(t) \end{bmatrix} \tag{44}$$

The external disturbances in the space robot control system are given as follows:

$$\boldsymbol{d} = \begin{bmatrix} 8 + 3\sin(0.25t) \\ 8 + 3\cos(0.25t) \\ 8 + 3\cos(0.25t) \end{bmatrix} \tag{45}$$

In addition, the nominal parts in dynamic of the space robot are defined as: $\boldsymbol{H}_0 = 0.8\boldsymbol{H}$ and $\boldsymbol{C}_0 = 0.8\boldsymbol{C}$. With the lumped disturbance $\boldsymbol{T}$ and disturbance compensation $\hat{\boldsymbol{T}}$ being defined, the estimation errors $\widetilde{\boldsymbol{T}}$ is given as $\widetilde{\boldsymbol{T}} = \boldsymbol{T} - \hat{\boldsymbol{T}}$.

To illustrate the effectiveness and feasibility of the proposed FASMDOB-based NFTSM control strategy, which converges tracking errors to the small neighbourhoods within a fixed time, a finite-time controller is introduced from [21], conducting the comparative simulations with the proposed fixed-time controller. The finite-time control system is defined as follows:

$$\begin{cases} \boldsymbol{s}_1 = \boldsymbol{a}\boldsymbol{e} + \boldsymbol{N}sig^{p/q}(\dot{\boldsymbol{e}}) \\ \tau_{eq} = \boldsymbol{H}_0(\hat{\boldsymbol{T}} + \ddot{\boldsymbol{q}}_d - \frac{q}{p}\boldsymbol{a}\boldsymbol{N}^{-1}sig^{2-p/q}(\dot{\boldsymbol{e}})) + \boldsymbol{C}_0\dot{\boldsymbol{q}} \\ \tau_{sw} = \boldsymbol{H}_0(-\boldsymbol{H}_{s1}\boldsymbol{s}_1 - \boldsymbol{H}_{s2}sig^{\rho_s}(\boldsymbol{s}_1) - \boldsymbol{H}_{s3}sig^{(|s_1|/|s_1(0)|)-\sigma_s}(\boldsymbol{s}_1)) \\ \tau_{FTC} = \tau_{eq} + \tau_{sw} \end{cases} \tag{46}$$

where $\boldsymbol{a} = diag\{a_1, \ldots, a_n\}$, $a_i > 1$, $\boldsymbol{N} = diag\{N_1, \ldots, N_n\}$, $N_i > 0$, p, q are positive odd constants with $1 < p/q < 2$. $\boldsymbol{H}_{s1} = diag\{H_{s11}, \ldots, H_{s1n}\}$, $H_{s1i} > 0$, $\boldsymbol{H}_{s2} = diag\{H_{s21}, \ldots, H_{s2n}\}$, $H_{s2i} > 0$, $\boldsymbol{H}_{s3} = diag\{H_{s31}, \ldots, H_{s3n}\}$, $H_{s3i} > 0$, $0 < \rho_s < 1$, $\sigma_s > 1$.

5.1. Case 1

To demonstrate the effectiveness of the proposed NFTSM control method, the following simulations are conducted in Case 1. Figure 3 describes the tracking performance of the proposed NFTSM controller under the initial state $\boldsymbol{e} = [-0.3, 0.3, 0.3]^{\mathrm{T}}$. Figure 4 represents the tracking errors of the proposed NFTSM control law. Figure 5 shows the control inputs of the proposed NFTSM controller. Figure 6 describes the approximation errors of the proposed FASMDOB and the finite-time disturbance observer [40] for the lumped disturbances. Figure 7 shows the approximation errors of FASMDOB with and without adaptive gain. Figure 8 shows the adaptive gain in the proposed FASMDOB.

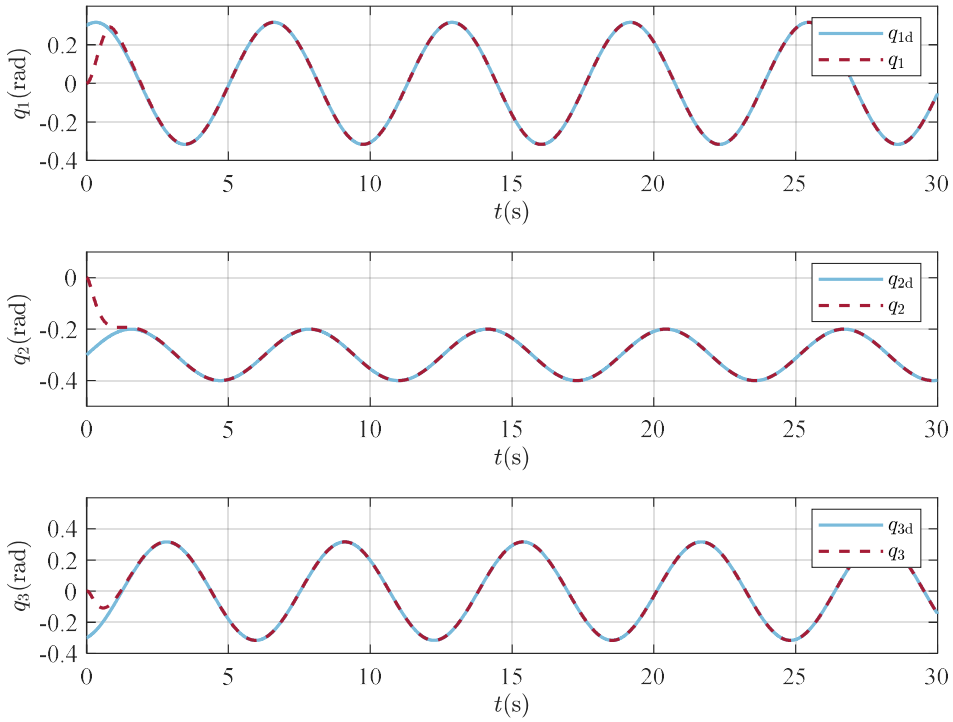

Figure 3. Tracking performances of proposed controller.

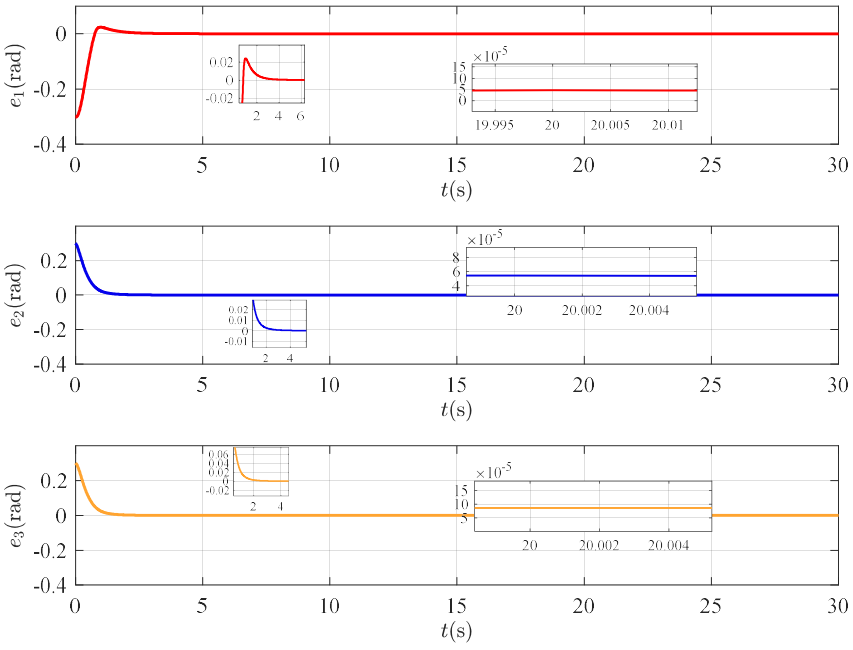

Figure 4. Tracking errors of proposed controller.

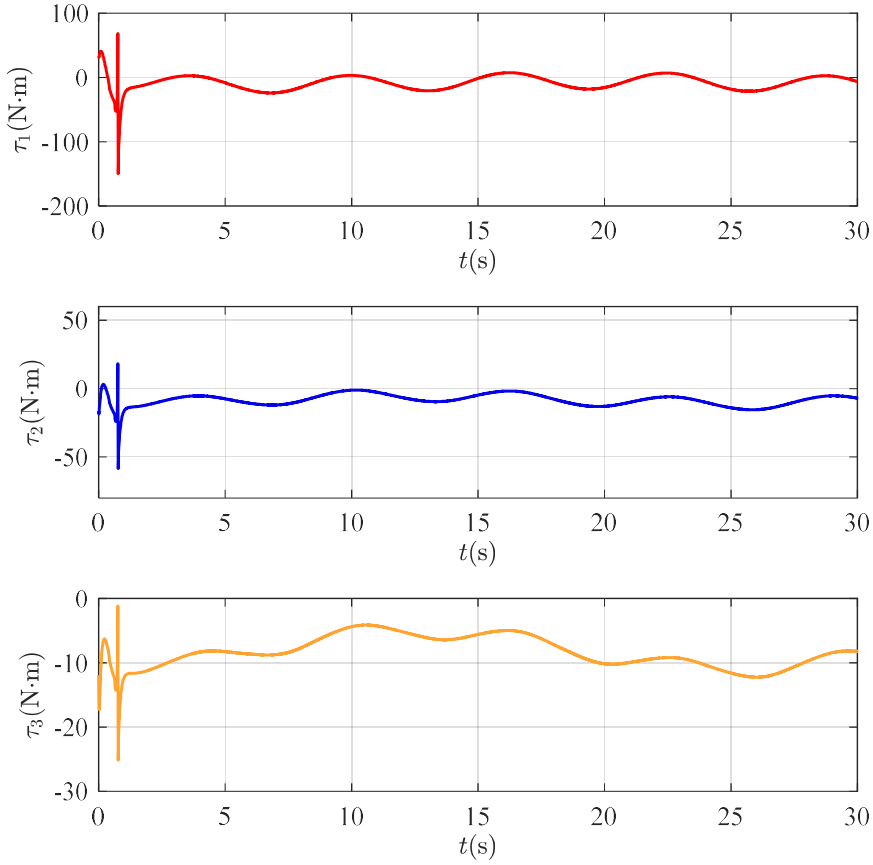

Figure 5. Control torques of proposed controller.

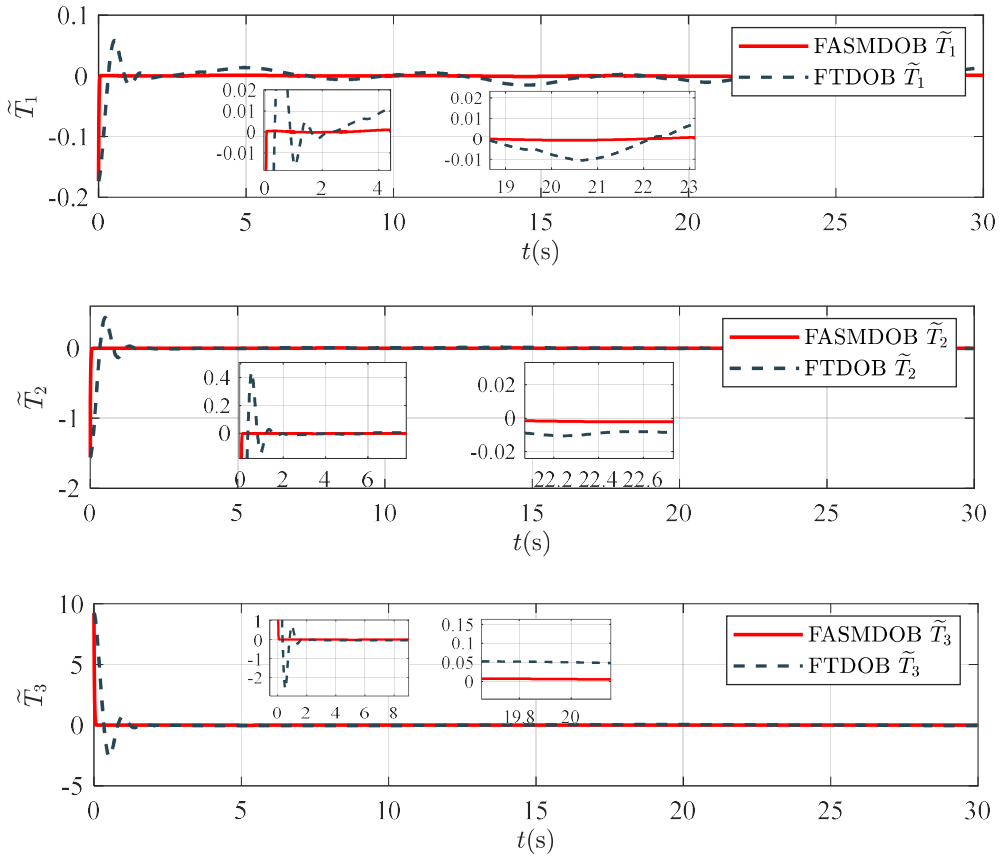

Figure 6. Disturbance approximation errors $\widetilde{T}$ of FASMDOB and FTDOB.

https://doi.org/10.3390/aerospace13060509

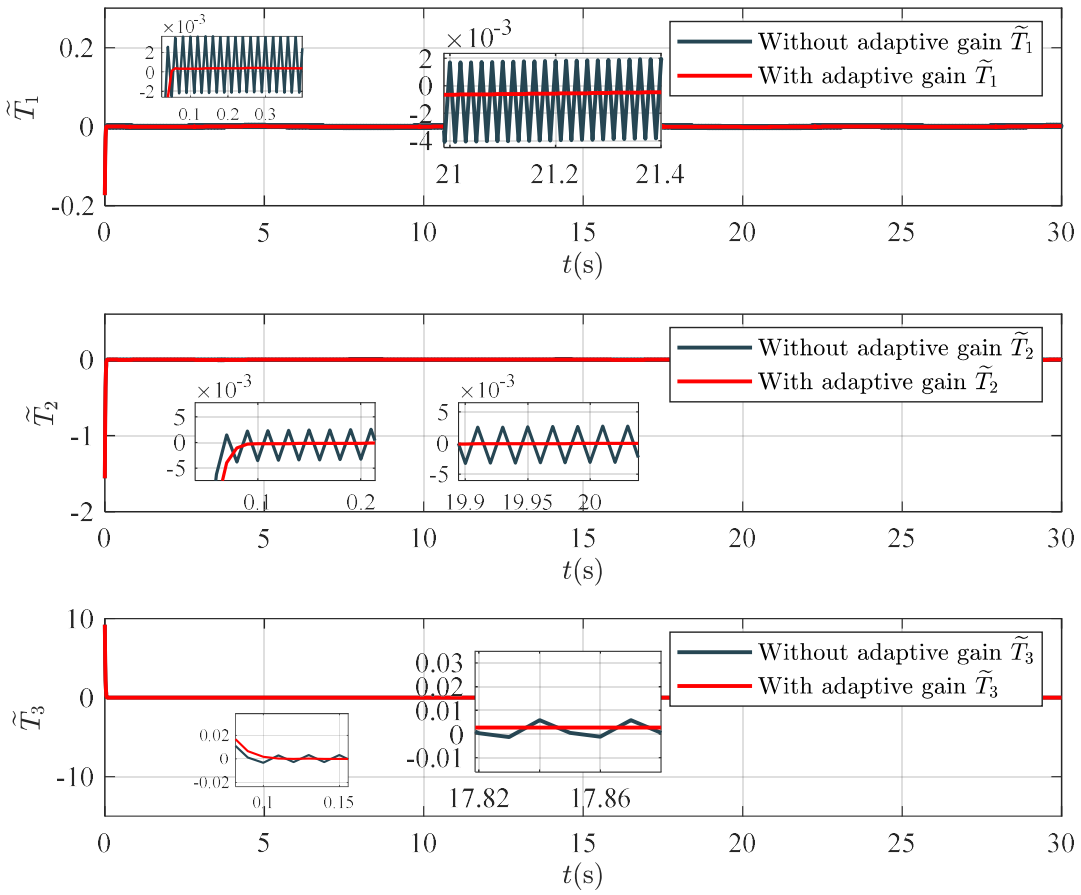

Figure 7. Approximation errors of FASMDOB with and without adaptive gain.

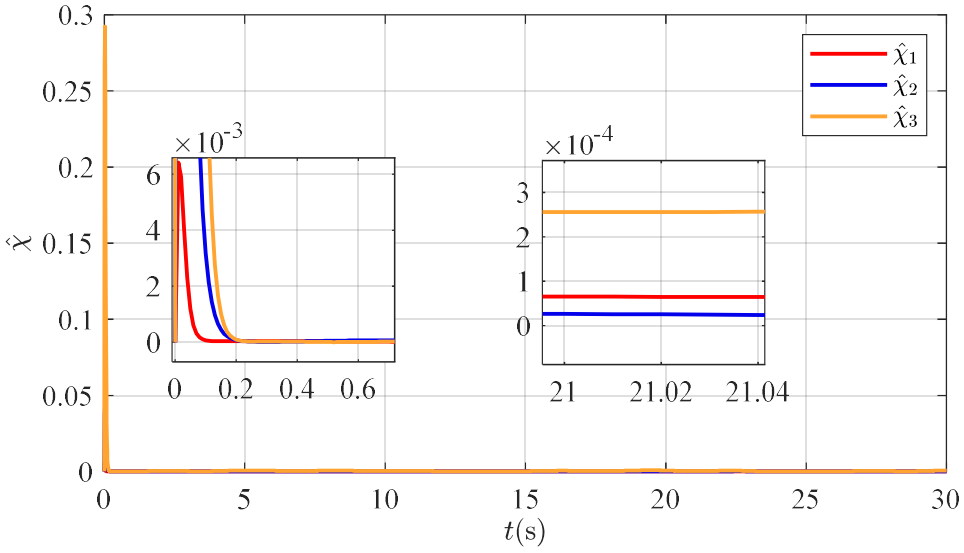

Figure 8. Adaptive gains of FASMDOB.

Figures 3 and 4 show the tracking performance of the proposed NFTSM controller under the initial state $\boldsymbol{e}(0) = [-0.3, 0.3, 0.3]^{\mathrm{T}}$. In Figure 4, it is observed that all tracking errors converge to zero with fixed time accurately. The convergence times of them are 3.49 s, 2.81 s and 2.79 s when tracking errors are within the bounds of 1×10^{-3}. The tracking accuracies of bases and joints can reach 1×10^{-5}, and the average tracking errors are given as 5.59×10^{-5}, 5.63×10^{-5} and 6.44×10^{-5}, which confirms the effectiveness of the proposed controller. Figure 5 describes the control inputs of the proposed NFTSM

controller under the initial state $\boldsymbol{e}(0) = [-0.3, 0.3, 0.3]^{\mathrm{T}}$. It can be seen that all control inputs remain within tolerable ranges, ensuring the feasibility of the proposed FXTC. The maximum control inputs are −149.716 N·m, −58.6195 N·m and −25.1937 N·m and the average control inputs are 10.1044 N·m, 8.0811 N·m and 8.0071 N·m in 5 s~30 s, which exhibits smooth energy consumption of the proposed controller.

Figure 6 describes the estimation performances of FASMDOB and FTDOB. Compared with FTDOB, since the maximum convergence time of FASMDOB only depends on the control parameters, the proposed FASMDOB has a faster convergence speed than FTDOB, where the maximum convergence time relies extremely on the initial states of the control system. The convergence times of the proposed FASMDOB are 0.05 s, 0.1 s and 0.12 s, while those of FTDOB are 2.25 s, 3.72 s and 1.89 s, which can negatively impact the tracking performance. Furthermore, the proposed FASMDOB has higher estimation accuracy; average estimation errors of FASMDOB are 4.3×10^{-4}, 5.1×10^{-4} and 2.8×10^{-3} in 10 s~30 s, while those of FTDOB only achieve 5.7×10^{-3}, 5.6×10^{-3} and 2.4×10^{-2}. Therefore, based on the above analysis, the proposed FASMDOB has more satisfactory compensation performances than FTDOB, showing its effectiveness in mitigating the impacts of the lumped disturbance on the trajectory tracking.

Figure 7 describes disturbance approximation errors of FASMDOB with and without adaptive gain. From the above figure, all approximation errors of both methods can converge to small regions within a fixed time. However, since FASMDOB with adaptive gain can dynamically adjust the gain of the switch function, the chattering of FASMDOB can be significantly mitigated, which enhances the estimation accuracy. The average estimation errors of the method without adaptive gain only approach 2.9×10^{-3}, 2.9×10^{-3} and 2.3×10^{-3} in 10 s~30 s, providing lower compensation accuracy than the method with adaptive gain. Furthermore, chattering in the method without adaptive gain can negatively impact the tracking performance and may even result in instability of the control system. Thus, the effectiveness of adaptive gain in FASMDOB has been validated.

Figure 8 describes the adaptive gain of FASMDOB $\hat{\chi}_i, i = 1, 2, 3$. From the above figure, the adaptive gains of FASMDOB converge with a fixed time and maintain at 1×10^{-3}, thereby resulting in the chattering reduction in FASMDOB. The convergence results of adaptive gains have further verified the effectiveness of the proposed FASMDOB.

5.2. Case 2

To verify the feasibility and effectiveness of the proposed FASMDOB-based NFTSM controller under arbitrary initial states, the following simulations are conducted with different initial states: $\boldsymbol{q}(0) = [0, 0, 0]^{\mathrm{T}}$, $\boldsymbol{q}(0) = [-0.2, 0.2, 0.2]^{\mathrm{T}}$ and $\boldsymbol{q}(0) = [-0.5, 0.5, 0.5]^{\mathrm{T}}$. Figure 9 depicts the tracking performance of the proposed NFTSM controller. Figure 10 shows the tracking errors of the proposed NFTSM controller, and Figure 11 shows the control torques of the proposed NFTSM controller under different initial states.

Figures 9 and 10 describe the tracking performances of the proposed NFTSM controller under different initial states. Since the maximum convergence time of the proposed FXTC only depends on the control parameters, all tracking errors rapidly converge to the small neighbourhoods with similar fixed time even under different initial states. The tracking accuracy of the base and joints all reach 1×10^{-5}. Figure 11 depicts control inputs of the proposed NFTSM controller under different initial states. As Figure 11 shows, all control inputs remain within appropriate ranges. The maximum control inputs are −272.475 N·m, −99.497 N·m and −50.331 N·m. Based on Figures 9–11, the feasibility and effectiveness of the proposed NFTSM controller even under different initial states are demonstrated.

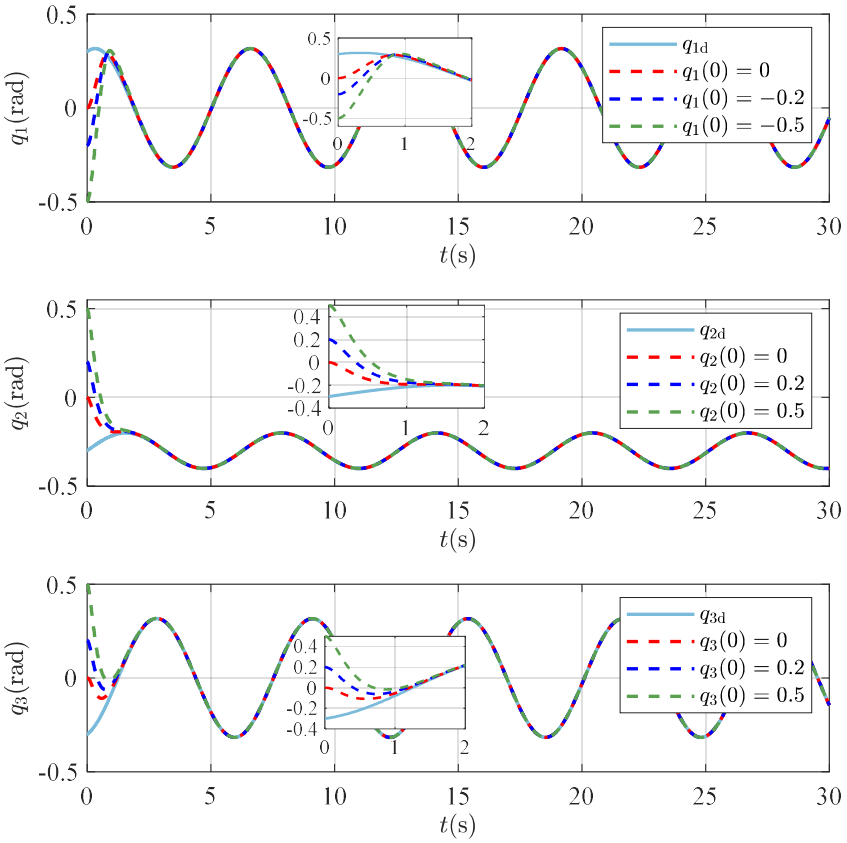

Figure 9. Tracking performances of proposed controller under different initial states.

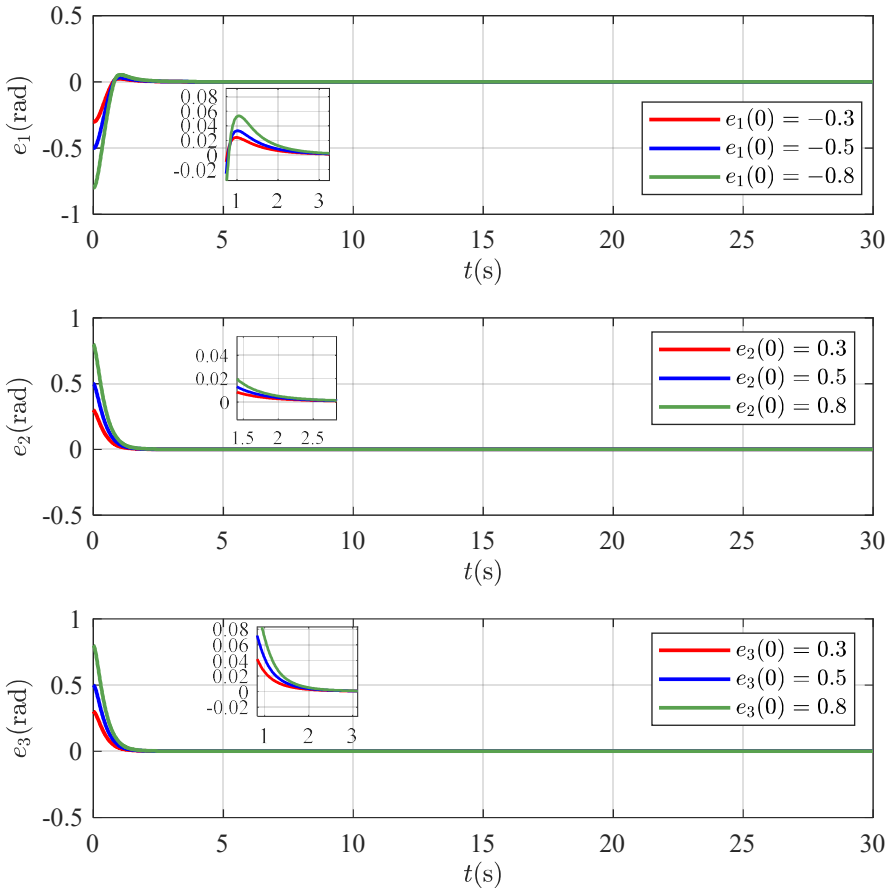

Figure 10. Tracking errors of proposed controller under different initial states.

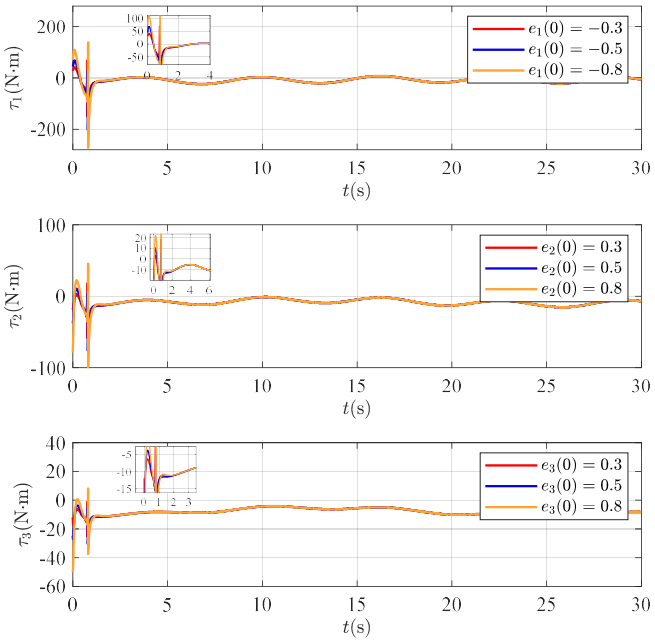

Figure 11. Control torques of proposed controller under different initial states.

5.3. Case 3

To verify the effectiveness of compensating for the lumped disturbance of FASMDOB in the proposed control system, the following comparative studies are depicted in Figures 12 and 13. Figure 12 shows the tracking performance of the control methods with FASMDOB and without FASMDOB under the same lumped disturbance $\boldsymbol{T}$ and initial states $\boldsymbol{e} = [-0.3, 0.3, 0.3]^{\mathrm{T}}$. Figure 13 depicts tracking errors of the control methods with FASMDOB and without FASMDOB.

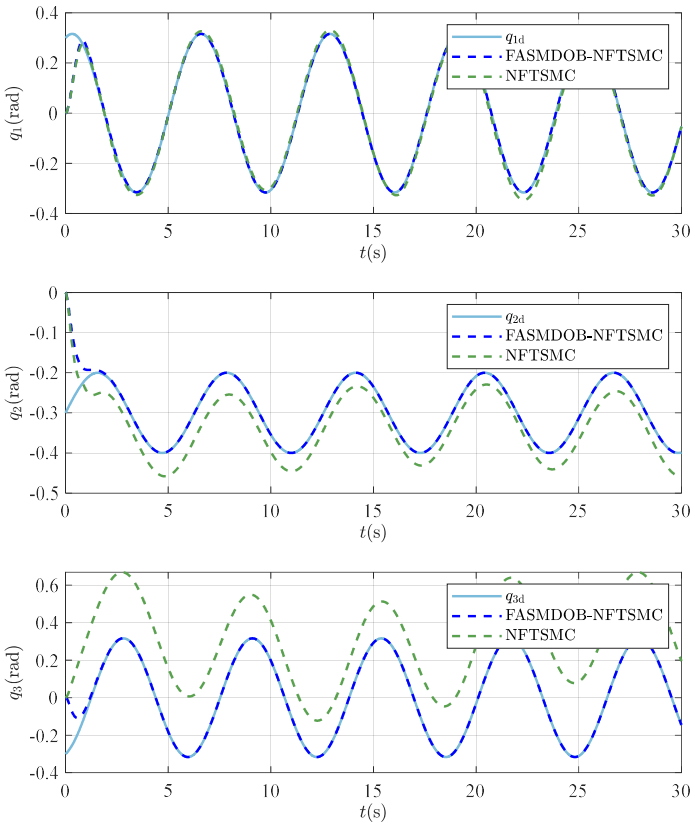

Figure 12. Tracking performances of FASMDOB-NFTSMC and NFTSMC.

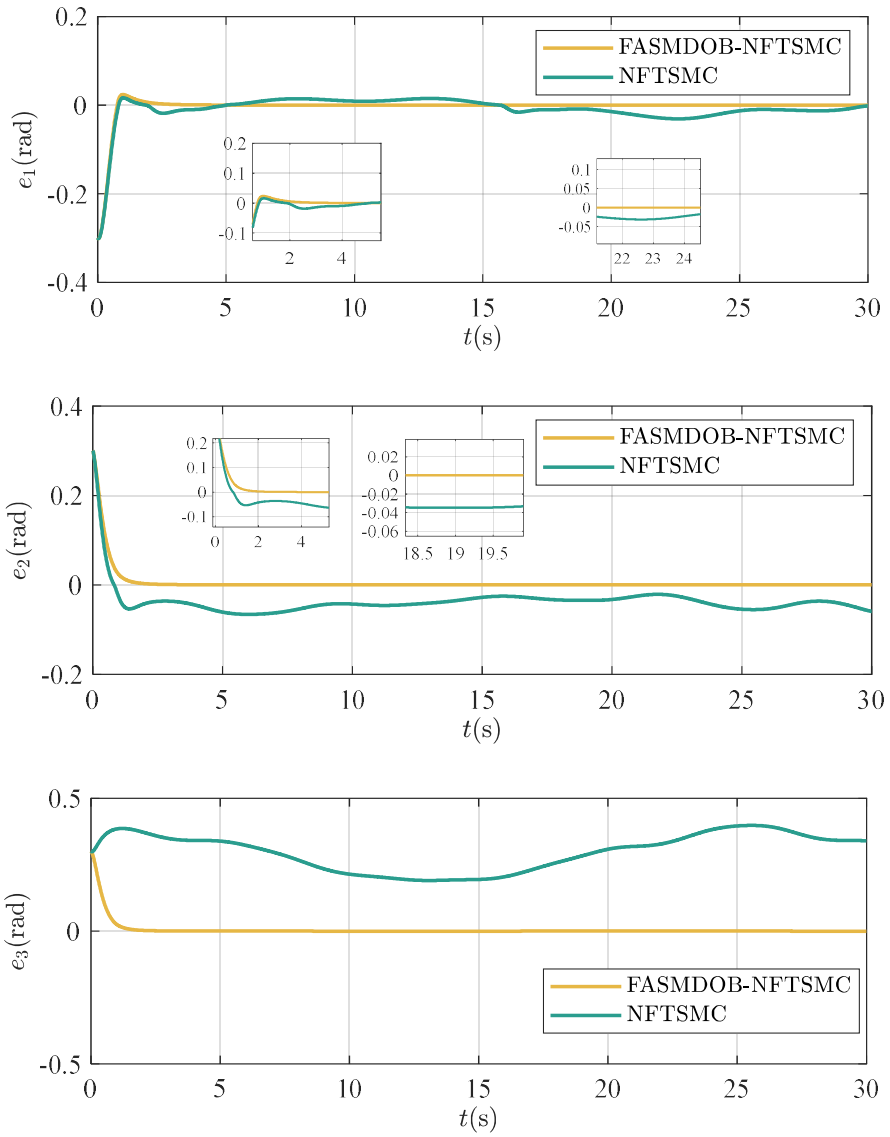

Figure 13. Tracking errors of FASMDOB-NFTSMC and NFTSMC.

Figure 13 describes tracking errors of FASMDOB-NFTSMC and NFTSMC. Based on the above figures, by utilizing FASMDOB to estimate the lumped disturbance, the proposed controller has effectively mitigated negative impacts from the disturbance, thereby enhancing control system performance. The average tracking errors of the NFTSM control method achieve 1.36×10^{-2}, 3.78×10^{-2} and 2.89×10^{-1}, while those of the FASMDOB-NFTSM control method achieve 5.59×10^{-5}, 5.63×10^{-5} and 6.44×10^{-5}. The above simulation results have demonstrated that FASMDOB can effectively compensate for the lumped disturbance.

5.4. Case 4

To demonstrate the effectiveness of the proposed FXTC strategy, an FTC method is introduced from [21] to conduct the following simulations. Figures 14 and 15 depict tracking performances of the proposed FXTC method and the FTC method [21] under the same initial states $\boldsymbol{q}(0) = [0, 0, 0]^{\mathrm{T}}$. Figure 14 presents the trajectory tracking of FXTC and FTC. Figure 15 describes the corresponding tracking errors of the proposed control method.

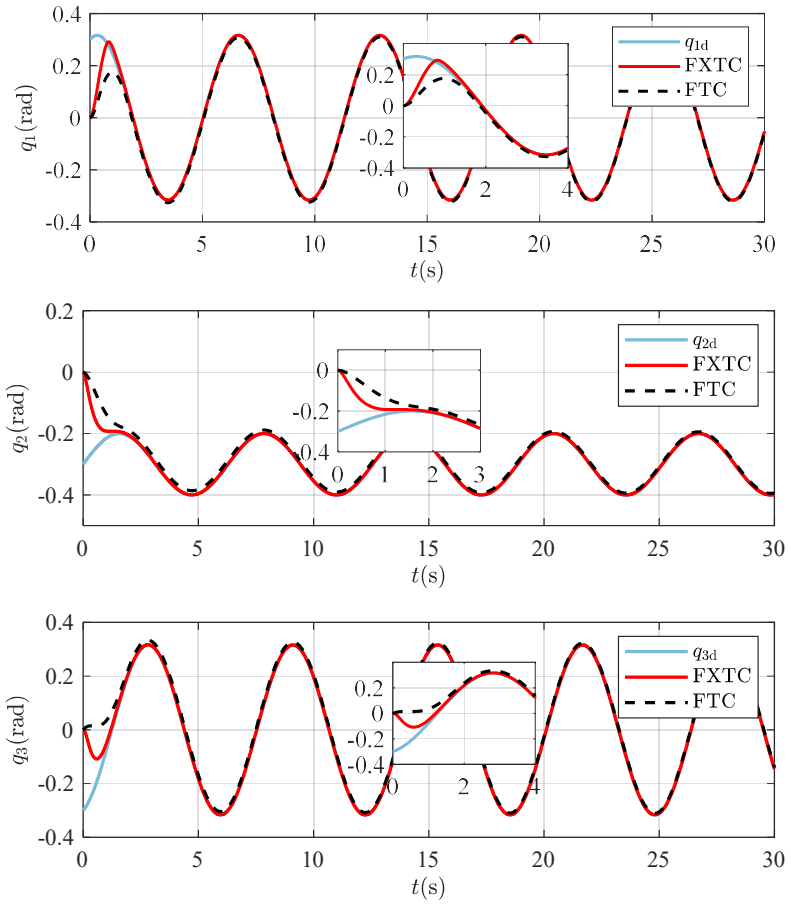

Figure 14. Tracking performances of the proposed FXTC and FTC [21].

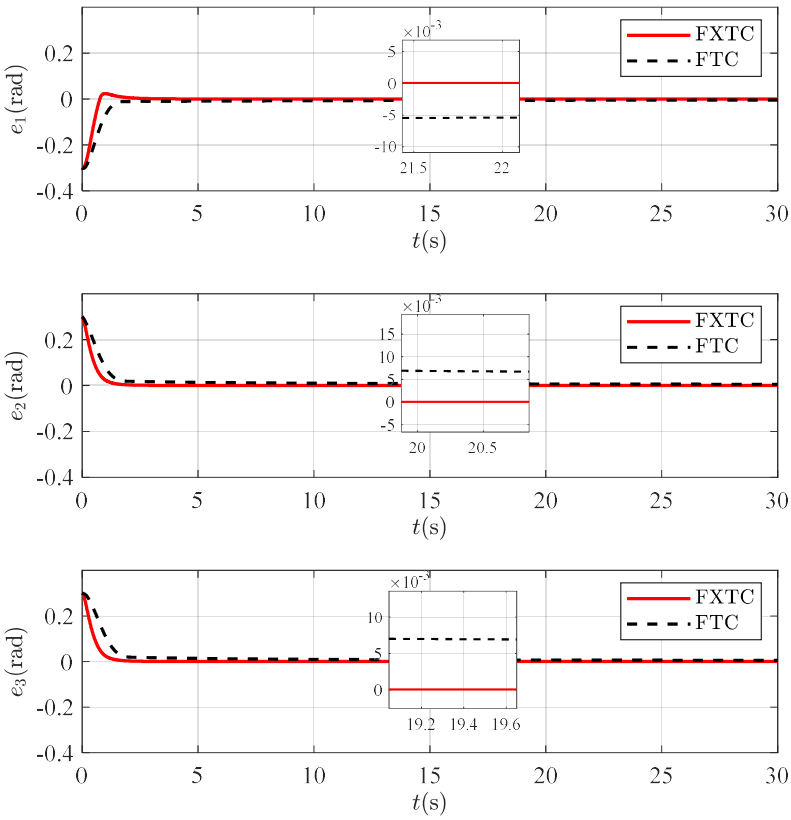

Figure 15. Tracking errors of the proposed FXTC and FTC [21].

Figure 14 represents the tracking performance of the proposed FXTC and FTC [21] under the same initial states $\boldsymbol{q}(0) = [0,0,0]^{\mathrm{T}}$. As the simulations depicted, both the proposed FXTC and FTC can achieve the goal of trajectory tracking for a space robot, driving the state variables to the equilibrium point with rapid convergence speeds. However, the convergence time of the proposed FXTC only depends on the control parameters, while the convergence time of the FTC relies on the initial states of the control system, which causes a longer convergence time. Thus, the proposed FXTC achieves faster convergence, 0.2 s~0.5 s, than the FTC. Figure 15 depicts the tracking errors of the proposed FXTC and FTC. The average tracking errors of the proposed FXTC reach 1×10^{-5}, while FTC [21] only achieves 1×10^{-3}. The convergence time with the NFTSMC method is 1.65 s, 1.35 s and 1.37 s, which is shorter than that of FTC at 3.22 s, 1.75 s and 1.99 s. As Figures 14 and 15 depict, the proposed NFTSMC has higher tracking accuracy and faster convergence speed than FTC, which directly demonstrates the key characteristic of fixed-time convergence in the proposed NFTSMC.

Figures 16 and 17 describe the tracking performance of the proposed FXTC and FXTNTSMC [37] under the initial states $\boldsymbol{e}(0) = [-0.3, 0.3, 0.3]^{\mathrm{T}}$. In Figure 17, all tracking errors of both methods converge to small neighbourhoods within a fixed time. Nonetheless, compared to FXTNTSMC, the proposed FXTC utilizes a novel reaching law, thereby achieving a faster convergence speed of tracking errors. The convergence times of the proposed FXTC are the same as the results in Case 1, while those of FXTNTSMC are 5.41 s, 5.34 s and 5.26 s, which are longer than the proposed FXTC. Furthermore, the proposed FXTC has higher tracking accuracy. The average tracking errors of FXTNTSMC are 4.48×10^{-4}, 4.43×10^{-4} and 4.84×10^{-4} in 10 s~30 s, while those of the proposed FXTC reach 1×10^{-5}. Therefore, based on the above figures, the proposed FXTC has more satisfactory transient and steady-state performance than the FXTNTSMC.

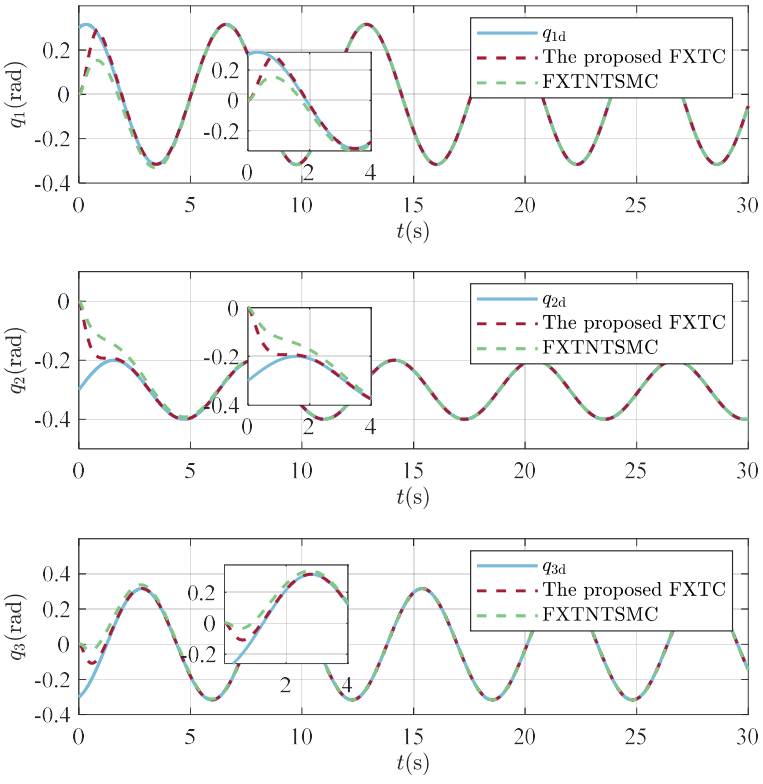

Figure 16. Tracking performance.

Figure 18 describes the estimation performance of the proposed FASMDOB and FXTDOB [21]. Since the proposed FASMDOB utilizes the adaptive technique to dynami-

cally adjust the gain of the switching function, the negative impacts from the chattering have been significantly mitigated. Therefore, it can be seen that the proposed FASMDOB has a faster convergence speed than FXTDOB. The convergence times of the FXTDOB are 1.45 s, 1.3 s and 0.6 s, while those of the proposed FASMDOB are 0.05 s, 0.1 s and 0.12 s. Moreover, compared to the proposed FASMDOB, the estimation errors of the FXTDOB exhibit severe overshoots and chattering, which can further degrade the estimation performance of the FXTDOB. Therefore, the average estimation errors of the FXTDOB are 9.2×10^{-3}, 5.7×10^{-3} and 2.4×10^{-2}, while those of the proposed FASMDOB are 4.3×10^{-4}, 5.1×10^{-4} and 2.8×10^{-3}. Based on the above figures, the effectiveness of the proposed FASMDOB is further verified and highlighted.

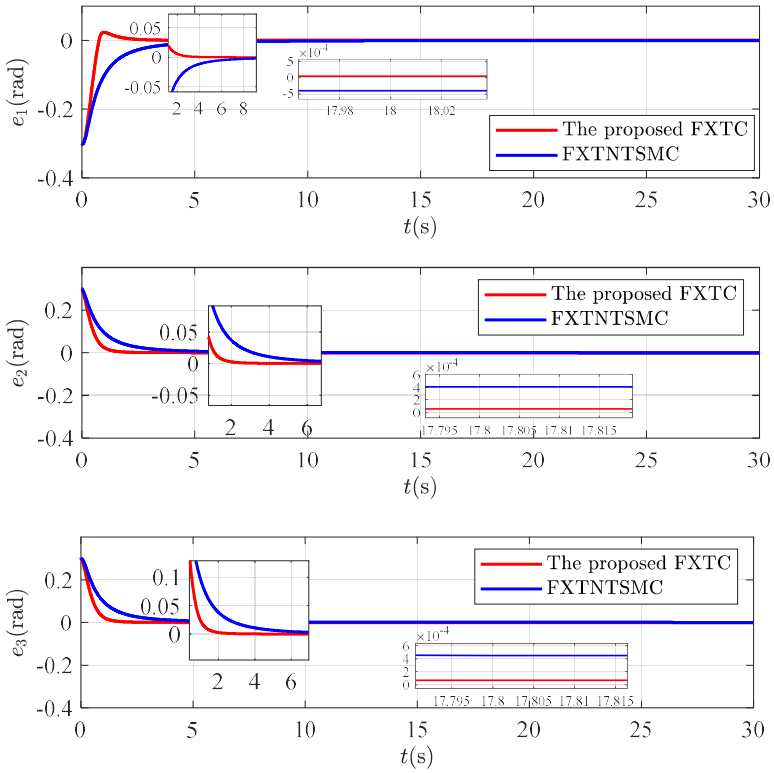

Figure 17. Tracking errors.

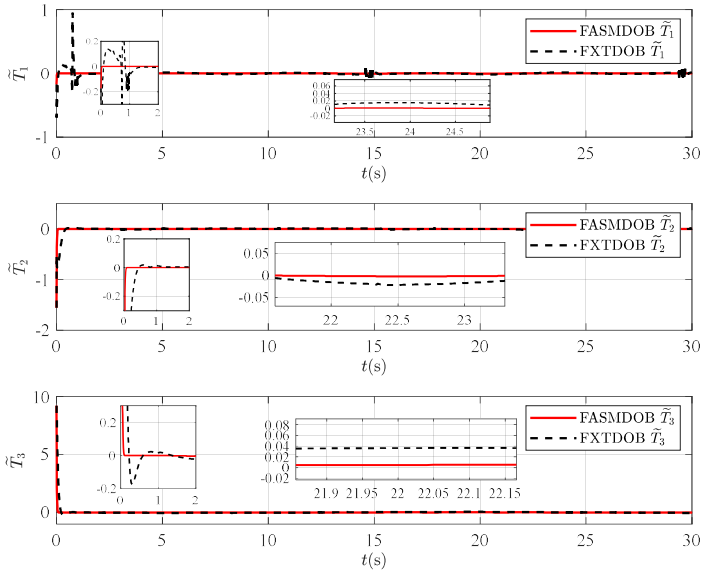

Figure 18. Approximation errors.

6. Conclusions

In this paper, an NFTSMC method with a novel reaching law is proposed to address the issue of trajectory tracking for uncertain space robot in the presence of external disturbance. The NFTSMC method involves a combination of NFTSM surface and FASMDOB. First, considering the adverse impacts from external disturbance and uncertain inertia parameters, a novel FASMDOB with an adaptive update law is proposed to estimate the lumped disturbance. Compared to FTDOB, FASMDOB achieves fixed-time convergence of observed disturbance and significantly mitigates the chattering in the observation results by using the adaptive update law. Next, a piecewise function-based NFTSM surface is proposed. By utilizing a piecewise function, the NFTSM surface effectively solves the singularity problem in conventional terminal sliding mode control. Based on the FASMDOB and NFTSM surface, the NFTSMC is proposed, which uses an arctangent function-based reaching law to enhance the performance of the control scheme. By using fixed-time Lyapunov theory, the stability of the proposed control system is proven. Lastly, several comparative simulations are conducted. As simulations show, the proposed control strategy can converge tracking errors to zero within a fixed time under arbitrary initial states, maintaining tracking accuracy with 1×10^{-5}. In addition, the proposed FASMDOB has faster convergence speed and higher estimation accuracy than FTDOB. Compared to the FTC, the FASMDOB-NFTSMC method enhances the tracking accuracy of space robot control systems from 1×10^{-3} to 1×10^{-5} and reduces the convergence time. Through the simulation results, the feasibility and effectiveness of FASMDOB-NFTSMC are demonstrated and highlighted. Although the proposed FXTC achieves fast convergence of tracking errors with high precision, there are some limitations in this study: the proposed FXTC method requires all state variables of the space robot system. However, obtaining all state variables of the space robot is challenging in applications, which could degrade control performance. Furthermore, the maximum convergence time of the proposed FXTC depends on a constant with a complex relationship to the control parameters, which may result in inaccurate convergence time. To address the above issues, an output feedback mechanism and a predefined-time control strategy can be introduced. Therefore, in the future work, the predefined-time control design with an output feedback mechanism will be taken into consideration.

Author Contributions: Conceptualization, H.A.; methodology, H.A. and A.Z.; software, Y.Y., Z.C. and X.F.; investigation, A.Z. and H.A.; writing—original draft preparation, Y.Y. and Z.C.; writing—review and editing H.A.; supervision, H.A. and X.F.; funding acquisition, H.A. and A.Z. All authors have read and agreed to the published version of the manuscript.

Funding: Jiangxi Provincial Natural Science Foundation under Grants 20232BAB212030, 20242BAB25258 and 20252BAC200187, the Jiangxi Provincial Key Laboratory of Particle Technology under Grants 20242BCC32119, and the Doctor research start-up fund of Jiangxi University of Science and Technology (205200100687).

Data Availability Statement: Data supporting results are included in the manuscript.

Conflicts of Interest: The authors declare no conflicts of interest.

Appendix A

Proof. First, taking the derivative of $\widehat{e}$, one can obtain the following:

$$\begin{aligned} \dot{\widehat{e}} &= \dot{\phi} - \dot{x}_2 \\ &= -\omega sig^{\delta}(\widehat{e}) - \zeta sig^{\vartheta}(\widehat{e}) - K_a \widehat{e} + \hat{T} - T \end{aligned} \tag{A1}$$

Substituting (A1) into (9), one yields:

$$\begin{aligned}\boldsymbol{\sigma} &= -\boldsymbol{\omega} sig^{\delta}(\widehat{\boldsymbol{e}}) - \boldsymbol{\zeta} sig^{\vartheta}(\widehat{\boldsymbol{e}}) - \boldsymbol{K}_a \widehat{\boldsymbol{e}} \\ &+\boldsymbol{\omega} sig^{\delta}(\widehat{\boldsymbol{e}}) + \boldsymbol{\zeta} sig^{\vartheta}(\widehat{\boldsymbol{e}}) + \boldsymbol{K}_a \widehat{\boldsymbol{e}} + \hat{\boldsymbol{T}} - \boldsymbol{T} \\ &= \hat{\boldsymbol{T}} - \boldsymbol{T}\end{aligned} \tag{A2}$$

Thus, based on (A2), the Lyapunov function V_{3i} is selected as follows:

$$V_{3i} = \frac{1}{2}\sigma_i^2 + \frac{\widetilde{\chi}_i^2}{2\mu_i} \tag{A3}$$

where $\widetilde{\chi}_i = \chi_i - \hat{\chi}_i$. Taking the derivative of V_1, one yields:

$$\dot{V}_{3i} = \sigma_i \dot{\sigma}_i - \frac{\widetilde{\chi}_i \dot{\hat{\chi}}_i}{\mu_i} \tag{A4}$$

Substituting (10) and (11) into (A4), the following equality is obtained:

$$\begin{aligned}\dot{V}_{3i} &= -\alpha_{si}|\sigma_i|^{\eta_i+1} - \beta_{si}|\sigma_i|^{\gamma_i+1} - K_{si}\sigma_i^2 - \hat{\chi}_i|\sigma_i| \\ &+k_{1i}\widetilde{\chi}_i\hat{\chi}_i - \widetilde{\chi}_i|\sigma_i| - \dot{T}_i\sigma_i\end{aligned} \tag{A5}$$

Based on Young's inequality, the following inequality is obtained:

$$k_{1i}\widetilde{\chi}_i\hat{\chi}_i \le -k_{1i}\widetilde{\chi}_i^2 + k_{1i}\chi_i^2 \tag{A6}$$

Substituting (A6) into (A5), (A5) can be reformulated as follows:

$$\begin{aligned}\dot{V}_{3i} &= -k_{1i}\widetilde{\chi}_i^2 + k_{1i}\chi_i^2 - \alpha_{si}|\sigma_i|^{\eta_i+1} - \beta_{si}|\sigma_i|^{\gamma_i+1} \\ &-K_{si}\sigma_i^2 - \hat{\chi}_i|\sigma_i| - \widetilde{\chi}_i|\sigma_i| - \dot{T}_i\sigma_i \\ &\le -k_{1i}\widetilde{\chi}_i^2 + k_{1i}\chi_i^2 - K_{si}\sigma_i^2 \\ &-\alpha_{si}|\sigma_i|^{\eta_i+1} - \beta_{si}|\sigma_i|^{\gamma_i+1} - (\left|\dot{T}_i\right| - \chi_i)|\sigma_i|\end{aligned} \tag{A7}$$

Based on Assumption 2, one obtains:

$$\begin{aligned}\dot{V}_{3i} &\le -k_{1i}\widetilde{\chi}_i^2 + k_{1i}\chi_i^2 - K_{si}\sigma_i^2 \\ &-\alpha_{si}|\sigma_i|^{\eta_i+1} - \beta_{si}|\sigma_i|^{\gamma_i+1}\end{aligned} \tag{A8}$$

Based on (A8), it can be seen that the proposed FASMDOB is stable. To further prove its fixed-time stability, (A8) can be reformed as follows:

$$\begin{aligned}\dot{V}_{3i} \le &-\alpha_{si}2^{\frac{\eta_i+1}{2}}(\tfrac{1}{2}\sigma_i^2)^{\frac{\eta_i+1}{2}} - \beta_{si}2^{\frac{\gamma_i+1}{2}}(\tfrac{1}{2}\sigma_i^2)^{\frac{\gamma_i+1}{2}} - K_{si}\sigma_i^2 - k_{1i}\widetilde{\chi}_i^2 - (\tfrac{1}{2}\widetilde{\chi}_i^2)^{\frac{\eta_i+1}{2}} \\ &-(\tfrac{1}{2}\widetilde{\chi}_i^2)^{\frac{\gamma_i+1}{2}} + ((\tfrac{1}{2}\widetilde{\chi}_i^2)^{\frac{\eta_i+1}{2}} + (\tfrac{1}{2}\widetilde{\chi}_i^2)^{\frac{\gamma_i+1}{2}} + k_{1i}\chi_i^2\end{aligned} \tag{A9}$$

$$\begin{aligned}\dot{V}_{3i} \le &-K_{v1}((\tfrac{1}{2}\sigma_i^2)^{\frac{\eta_i+1}{2}} + (\tfrac{1}{2}\widetilde{\chi}_i^2)^{\frac{\eta_i+1}{2}}) - K_{v2}((\tfrac{1}{2}\sigma_i^2)^{\frac{\gamma_i+1}{2}} + (\tfrac{1}{2}\widetilde{\chi}_i^2)^{\frac{\gamma_i+1}{2}}) \\ &-K_{v3}((\tfrac{1}{2}\sigma_i^2) + (\tfrac{1}{2}\widetilde{\chi}_i^2)) + \Pi_s\end{aligned} \tag{A10}$$

where K_{v1}, K_{v2}, K_{v3} are defined as $K_{v1} = \min(\alpha_{si}2^{\frac{\eta_i+1}{2}}, 1)$, $K_{v2} = \min(\beta_{si}2^{\frac{\gamma_i+1}{2}}, 1)$, $K_{v3} = \min(2K_{si}, 2k_{1i})$. $\Pi_s = (\frac{1}{2}\widetilde{\chi}_i^2) + (\frac{1}{2}\widetilde{\chi}_i^2)^{\frac{\eta_i+1}{2}} + (\frac{1}{2}\widetilde{\chi}_i^2)^{\frac{\gamma_i+1}{2}} + k_{1i}\chi_i^2$.

According to Lemma 2, (A10) can be transformed into the following:

$$\dot{V}_{3i} \le -K_{v4}V_{3i}^{\frac{\eta_i+1}{2}} - K_{v2}V_{3i}^{\frac{\gamma_i+1}{2}} - K_{v3}V_{3i} + \Pi_s \tag{A11}$$

where $K_{v4} = 2^{1-\frac{\eta_i+1}{2}} K_{v1}$.

To verify fixed-time convergence of FASMDOB, (A11) can be transformed into three forms:

$$\dot{V}_{3i} \leq -(1-\rho_v)K_{v3}V_{3i} - \rho_v K_{v3}V_{3i} - K_{v4}V_{3i}^{\frac{\eta_i+1}{2}} - K_{v2}V_{3i}^{\frac{\gamma_i+1}{2}} + \Pi_s \tag{A12}$$

$$\dot{V}_{3i} \leq -K_{v3}V_{3i} - (1-\rho_v)K_{v4}V_{3i}^{\frac{\eta_i+1}{2}} - \rho_v K_{v4}V_{3i}^{\frac{\eta_i+1}{2}} - K_{v2}V_{3i}^{\frac{\gamma_i+1}{2}} + \Pi_s \tag{A13}$$

$$\dot{V}_{3i} \leq -K_{v3}V_{3i} - K_{v4}V_{3i}^{\frac{\eta_i+1}{2}} - (1-\rho_v)K_{v2}V_{3i}^{\frac{\gamma_i+1}{2}} - \rho_v K_{v2}V_{3i}^{\frac{\gamma_i+1}{2}} + \Pi_s \tag{A14}$$

where $\rho_v > 0$.

Considering (A13), when $-(1-\rho_v)K_{v4}V_{3i}^{\frac{\eta_i+1}{2}} + \Pi_s \leq 0$, (A13) can be transformed into the following inequality:

$$\dot{V}_{3i} \leq -K_{v3}V_{3i} - \rho_v K_{v4}V_{3i}^{\frac{\eta_i+1}{2}} - K_{v2}V_{3i}^{\frac{\gamma_i+1}{2}} \tag{A15}$$

Solving the differential inequality (A15), the convergence time of FASMDOB T_{v2} is defined as follows:

$$T_{v2} \leq \frac{2\ln(1+\frac{K_{v3}}{K_{v2}})}{K_{v3}(\gamma_i-1)} + \frac{2}{\rho_v K_{v4}(1-\eta_i)} \tag{A16}$$

Conducting a similar analysis to (A12) and (A14), we can obtain the maximum convergence time T_v:

$$T_v \leq \max(T_{v1}, T_{v2}, T_{v3}) \tag{A17}$$

where $T_{v1} = \frac{2\ln(1+\frac{\rho_v K_{v3}}{K_{v2}})}{\rho_v K_{v3}(\gamma_i-1)} + \frac{2}{K_{v4}(1-\eta_i)}$ and $T_{v3} = \frac{2\ln(1+\frac{K_{v3}}{\rho_v K_{v2}})}{K_{v3}(\gamma_i-1)} + \frac{2}{K_{v4}(1-\eta_i)}$.

The convergence region of FASMDOB is defined as follows:

$$\Omega_{vi} = \left\{ \lim_{t\to T_v} \sigma_i \;\middle|\; |\sigma_i| \leq \min\left\{ \sqrt{2\left(\frac{\Pi_s}{K_{v3}(1-\rho_v)}\right)}, \sqrt{2\left(\frac{\Pi_s}{K_{v4}(1-\rho_v)}\right)^{\frac{2}{\eta_i+1}}}, \sqrt{2\left(\frac{\Pi_s}{K_{v2}(1-\rho_v)}\right)^{\frac{2}{\gamma_i+1}}} \right\} \right\} \tag{A18}$$

Based on the above analysis, the proposed FASMDOB can converge estimation errors of the lumped disturbance to a small region within a fixed time. The validity of Theorem 1 is demonstrated. □

References

1. Son, J.; Kang, H.; Kim, M.; Lee, J.; Kang, S.H. Robust Adaptive PID Control Based on a Modified Nussbaum Function for Robots Exposed to Significant Changes in Dynamics. *IEEE/ASME Trans. Mechatron.* **2026**, *early access*. [CrossRef]
2. Han, J.; Shan, X.; Liu, H.; Xiao, J.; Huang, T. Fuzzy gain scheduling PID control of a hybrid robot based on dynamic characteristics. *Mech. Mach. Theory* **2023**, *184*, 105283. [CrossRef]
3. Liu, F.; Liu, W.; Luo, H. Operational stability control of a buried pipeline maintenance robot using an improved PSO-PID controller. *Tunn. Undergr. Space Technol.* **2023**, *138*, 105178. [CrossRef]
4. Xie, S.; Sun, W.; Sun, Y.; Su, S.-F. Adaptive prescribed-time optimal control for flexible-joint robots via reinforcement learning. *IEEE Trans. Syst. Man Cybern. Syst.* **2025**, *55*, 2633–2643. [CrossRef]
5. Prakash, R.; Behera, L.; Jagannathan, S. Adaptive critic optimal control of an uncertain robot manipulator with applications. *IEEE Trans. Control Syst. Technol.* **2024**, *33*, 316–326. [CrossRef]
6. Yang, T.; Lu, Z.; Cui, G. Low-Complexity Predefined-Time Optimal Safe Formation Control for Nonholonomic Mobile Robot via Funnel Technique. *IEEE Internet Things J.* **2025**, *13*, 4782–4791. [CrossRef]
7. Van, M.; Sun, Y.; Mcllvanna, S.; Nguyen, M.-N.; Khyam, M.O.; Ceglarek, D. Adaptive fuzzy fault tolerant control for robot manipulators with fixed-time convergence. *IEEE Trans. Fuzzy Syst.* **2023**, *31*, 3210–3219. [CrossRef]
8. Brahmi, B.; Ghommam, J.; Saad, M. Disturbance observer-based backstepping-super twisting control for robust trajectory tracking in robot manipulators. *IEEE/ASME Trans. Mechatron.* **2025**, *30*, 5686–5697. [CrossRef]

9. Chen, J.; Hua, C.; Mu, D.; Sun, F. Lyapunov-Based Adaptive Neural Network Optimized Backstepping Control of Uncertain Unmanned Fire Fighting Robot. *IEEE Trans. Intell. Transp. Syst.* **2025**, *26*, 12014–12024. [CrossRef]
10. Adane, A.G.; Abdissa, C.M. Adaptive fuzzy sliding mode controller of three link robot arm manipulator. *IEEE Access* **2025**, *13*, 158222–158236. [CrossRef]
11. Fu, X.; Ai, H.; Chen, L. Integrated sliding mode control with input restriction, output feedback and repetitive learning for space robot with flexible-base, flexible-link and flexible-joint. *Robotica* **2023**, *41*, 370–391. [CrossRef]
12. Zhu, A.; Ai, H.; Chen, L. FSTSMC compliance control for dual-arm space robot with SDBD capture satellite operation. *J. Comput. Nonlinear Dyn.* **2023**, *18*, 061006. [CrossRef]
13. Song, T.; Fang, L.; Zhang, Y.; Shen, H. Recursive terminal sliding mode based control of robot manipulators with a novel sliding mode disturbance observer. *Nonlinear Dyn.* **2024**, *112*, 1105–1121. [CrossRef]
14. Tavoosi, S.; Siahi, M.; Soltanpour, M.R.; Moarefianpour, A. Fault-tolerant terminal sliding mode control of flexible joint manipulators based on fault detection and estimation. *J. Braz. Soc. Mech. Sci. Eng.* **2025**, *47*, 223. [CrossRef]
15. Zhao, S.; Wang, S.; Li, J.; Han, G.; He, Y.; Chen, H.; Luo, W.; Sun, Y. Fuzzy second-order integral terminal adaptive sliding mode control for marine cable-driven parallel grinding robot. *Ocean Eng.* **2025**, *326*, 120784. [CrossRef]
16. Yang, P.; Zhang, S.; Yu, X.; He, W. Reinforcement-learning-based finite time fault tolerant control for a manipulator with actuator faults. *IEEE Trans. Cybern.* **2025**, *55*, 2621–2632. [CrossRef] [PubMed]
17. Li, X.-F.; Wang, J.; Zhang, H.-Y.; Zhang, K.-W.; Lu, G.-D. Adaptive composite observer-based global finite time control with prescribed performance for robots. *IEEE Trans. Ind. Electron.* **2023**, *71*, 9351–9363. [CrossRef]
18. Zhang, T.; Shi, P.; Li, W.; Yue, X. Discrete nonsingular terminal sliding mode control for trajectory tracking of space manipulators with mismatched multiple disturbances and noisy measurements. *Aerosp. Sci. Technol.* **2024**, *144*, 108766. [CrossRef]
19. Zheng, S.; Zha, Y.; Ahn, C.K.; Lu, S.; Song, B. Constrained finite-time output regulation for robot manipulators with control input delay. *IEEE/ASME Trans. Mechatron.* **2025**, *30*, 6654–6666. [CrossRef]
20. Li, Y.; Dong, S.; Li, K. Fuzzy adaptive finite-time event-triggered control of time-varying formation for nonholonomic multirobot systems. *IEEE Trans. Intell. Veh.* **2023**, *9*, 725–737. [CrossRef]
21. Wang, Y.; Jiao, W. Fixed-Time Disturbance Observer-Based Terminal Sliding Mode Control for Manipulators with a Novel Reaching Law. *IEEE Access* **2024**, *12*, 105766–105777. [CrossRef]
22. Zhu, C.; Jiang, Y.; Yang, C. Fixed-time neural control of robot manipulator with global stability and guaranteed transient performance. *IEEE Trans. Ind. Electron.* **2022**, *70*, 803–812. [CrossRef]
23. Wang, C.; Zhan, H.; Guo, Q.; Li, T. Adaptive dynamic programming-based fixed-time optimal control for wheeled mobile robot. *IEEE Robot. Autom. Lett.* **2024**, *10*, 176–183. [CrossRef]
24. Qi, X.; Xu, S.; Li, Y.; Chu, Y. Global fixed-time event-triggered control for stochastic nonlinear systems with full state constraints. *Nonlinear Dyn.* **2023**, *111*, 7403–7415. [CrossRef]
25. Ai, H.; Zheng, Y.; Xu, Z.; Jiang, L.; Zhu, A.; Fu, X. Bounded Barrier Lyapunov Function-Based Neural Network Control of Space Robot with Output Tracking Error Constraints and Input Saturation. *ISA Trans.* **2026**, *173*, 220–234. [CrossRef]
26. Yun, C.-G.; Pak, S.-J.; Sin, Y.-C.; Rim, C.-M. Trajectory tracking control of a four-wheeled omnidirectional mobile robot using computed torque control and radial basis function neural network. *J. Braz. Soc. Mech. Sci. Eng.* **2026**, *48*, 336. [CrossRef]
27. Zong, L.; Jiang, C.; Du, H.; Luo, Y.; Cong, Y. Interaction force control of industrial manipulators via neural network-based integral terminal sliding mode control algorithm. *Nonlinear Dyn.* **2025**, *113*, 26361–26375. [CrossRef]
28. Ding, W.; Zhang, J.X.; Shi, P. Adaptive fuzzy control of wheeled mobile robots with prescribed trajectory tracking performance. *IEEE Trans. Fuzzy Syst.* **2024**, *32*, 4510–4521. [CrossRef]
29. Duong, M.-D.; Pham, Q.-T.; Vu, T.-C.; Bui, N.-T.; Dao, Q.-T. Adaptive fuzzy sliding mode control of an actuator powered by two opposing pneumatic artificial muscles. *Sci. Rep.* **2023**, *13*, 8242. [CrossRef]
30. Dong, H.; Sun, W.; Zhu, C. Adaptive Fuzzy Tracking Control for Flexible-Joint Robots with Random Disturbances and Unknown Measurement Sensitivity. *Int. J. Fuzzy Syst.* **2025**, *27*, 2441–2454. [CrossRef]
31. Yin, M.; Wang, H.; Shang, D.; Li, M.; Xu, T.; Wu, X. Disturbance compensation control for humanoid robot hand driven by tendon-sheath based on disturbance observer. *IEEE Trans. Autom. Sci. Eng.* **2025**, *22*, 13387–13397. [CrossRef]
32. Wei, T.; Liao, Y.; Wan, L.; Yang, C.; Zhang, T.; Zhang, M. A Disturbance Rejection Scheme for ASR Heading Control Based on an Improved Extended State Observer and Experiment Research. *IEEE Trans. Autom. Sci. Eng.* **2025**, *22*, 22384–22395. [CrossRef]
33. Sun, Z.; Li, Z.; Wu, G.; Zheng, J.; Man, Z. Sliding mode-based actuator fault reconstruction and fault-tolerant control of lower limb rehabilitation exoskeleton robots. *Control Eng. Pract.* **2026**, *167*, 106659. [CrossRef]
34. Qiang, J.; Li, L.; Hua, C.; Ren, X.; Liu, C. Fixed-Time Generalized VGESO-Based Trajectory Tracking Control for WMRs on Uneven Road: A Fully Actuated System Approach. *IEEE Trans. Circuits Syst. I Regul. Pap.* **2025**, *72*, 2915–2927. [CrossRef]
35. Vo, A.T.; Truong, T.N.; Le, Q.D.; Kang, H.-J. Fixed-time sliding mode-based active disturbance rejection tracking control method for robot manipulators. *Machines* **2023**, *11*, 140. [CrossRef]

36. Jin, X.; Jiang, J.; Qin, J.; Zheng, W.X.; Gao, M. Observer-based fixed-time-synchronized control for uncertain Euler–Lagrange systems with bias–actuator faults. *IEEE Trans. Cybern.* **2025**, *55*, 3811–3824. [CrossRef]
37. Liu, W.; Liu, L.; Zhang, D.; Cheng, J. Nonsingular fast terminal sliding mode control of uncertain robotic manipulator system based on adaptive fuzzy wavelet neural network. *Int. J. Fuzzy Syst.* **2025**, *27*, 898–911. [CrossRef]
38. Ji, W.; Chen, H.; Qiu, J.; Fan, Y. Output Feedback Asynchronous Fuzzy SMC of Nonlinear Markov Jump Systems via Hidden Mode Detections. *IEEE Trans. Syst. Man Cybern. Syst.* **2026**, *56*, 3049–3059. [CrossRef]
39. Ji, W.; Zhang, H.; Qiu, J. Further results on asynchronous fuzzy observer-based output feedback control for networked nonlinear systems using quantized measurements. *IEEE Trans. Syst. Man Cybern. Syst.* **2024**, *54*, 5556–5566. [CrossRef]
40. Cao, P.; Gan, Y.; Dai, X. Finite-time disturbance observer for robotic manipulators. *Sensors* **2019**, *19*, 1943. [CrossRef]